

# Leukocyte Complexity Predicts Breast Cancer Survival and Functionally Regulates Response to Chemotherapy

David G. DeNardo<sup>1</sup>, Donal J. Brennan<sup>2</sup>, Elton Rexhepaj<sup>2</sup>, Brian Ruffell<sup>1</sup>, Stephen L. Shiao<sup>3</sup>, Stephen F. Madden<sup>4</sup>, William M. Gallagher<sup>2</sup>, Nikhil Wadhvani<sup>1</sup>, Scott D. Keil<sup>1</sup>, Sharfaa A. Junaid<sup>1</sup>, Hope S. Rugo<sup>5,6</sup>, E. Shelley Hwang<sup>6,7</sup>, Karin Jirstrom<sup>8</sup>, Brian L. West<sup>9</sup>, and Lisa M. Coussens<sup>1,5</sup>

## ABSTRACT

Immune-regulated pathways influence multiple aspects of cancer development. In this article we demonstrate that both macrophage abundance and T-cell abundance in breast cancer represent prognostic indicators for recurrence-free and overall survival. We provide evidence that response to chemotherapy is in part regulated by these leukocytes; cytotoxic therapies induce mammary epithelial cells to produce monocyte/macrophage recruitment factors, including colony stimulating factor 1 (CSF1) and interleukin-34, which together enhance CSF1 receptor (CSF1R)-dependent macrophage infiltration. Blockade of macrophage recruitment with CSF1R-signaling antagonists, in combination with paclitaxel, improved survival of mammary tumor-bearing mice by slowing primary tumor development and reducing pulmonary metastasis. These improved aspects of mammary carcinogenesis were accompanied by decreased vessel density and appearance of antitumor immune programs fostering tumor suppression in a CD8<sup>+</sup> T-cell-dependent manner. These data provide a rationale for targeting macrophage recruitment/response pathways, notably CSF1R, in combination with cytotoxic therapy, and identification of a breast cancer population likely to benefit from this novel therapeutic approach.

**SIGNIFICANCE:** These findings reveal that response to chemotherapy is in part regulated by the tumor immune microenvironment and that common cytotoxic drugs induce neoplastic cells to produce monocyte/macrophage recruitment factors, which in turn enhance macrophage infiltration into mammary adenocarcinomas. Blockade of pathways mediating macrophage recruitment, in combination with chemotherapy, significantly decreases primary tumor progression, reduces metastasis, and improves survival by CD8<sup>+</sup> T-cell-dependent mechanisms, thus indicating that the immune microenvironment of tumors can be reprogrammed to instead foster antitumor immunity and improve response to cytotoxic therapy. *Cancer Discovery*; 1(1); 54-67. ©2011 AACR.

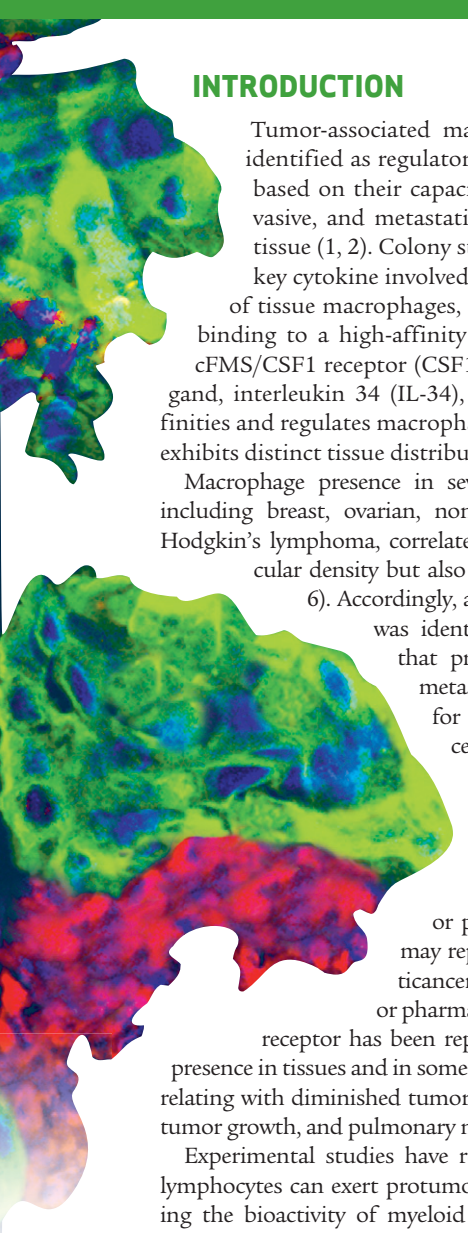
**Authors' Affiliations:** <sup>1</sup>Departments of Pathology, <sup>3</sup>Radiation Oncology, <sup>5</sup>Medicine, and <sup>7</sup>Surgery, and <sup>6</sup>Helen Diller Family Comprehensive Cancer Center, University of California, San Francisco; <sup>2</sup>University College Dublin School of Biomolecular and Biomedical Science, University College Dublin Conway Institute, Belfield, and <sup>4</sup>National Institute for Cellular Biotechnology, Dublin City University, Glasnevin, Dublin, Ireland; <sup>8</sup>Center for Molecular Pathology, Department of Laboratory Medicine, Lund University, Skåne University Hospital, Malmö, Sweden; and <sup>9</sup>Plexikon Inc., Berkeley, California  
Current affiliation for Dr. DeNardo: Department of Medicine, Washington University, St. Louis, Missouri

**Note:** Supplementary data for this article are available at Cancer Discovery Online (<http://www.aacrjournals.org>).

**Corresponding Author:** Lisa M. Coussens, Department of Pathology, University of California, San Francisco, 513 Parnassus Avenue, HSW450C, San Francisco, CA 94143. Phone: 415-502-6318; Fax: 415-514-0878; E-mail: [Lisa.Coussens@ucsf.edu](mailto:Lisa.Coussens@ucsf.edu)

doi: 10.1158/2159-8274.CD-10-0028

©2011 American Association for Cancer Research.



## INTRODUCTION

Tumor-associated macrophages (TAM) have been identified as regulators of solid tumor development based on their capacity to enhance angiogenic, invasive, and metastatic programming of neoplastic tissue (1, 2). Colony stimulating factor-1 (CSF1) is a key cytokine involved in recruitment and activation of tissue macrophages, exerting these effects through binding to a high-affinity receptor tyrosine kinase, the cFMS/CSF1 receptor (CSF1R; ref. 3). A second CSF1R ligand, interleukin 34 (IL-34), possesses similar binding affinities and regulates macrophage recruitment to tissues, but exhibits distinct tissue distribution characteristics (4).

Macrophage presence in several types of human cancer, including breast, ovarian, non-small cell lung cancer, and Hodgkin's lymphoma, correlates not only with increased vascular density but also a worse clinical outcome (1, 5, 6). Accordingly, a CSF1-response gene signature was identified in human breast cancer that predicts risk of recurrence and metastasis, and is similarly predictive for clinical outcome in colon cancer and leiomyosarcoma (7-9).

On the basis of these findings, it seems reasonable to postulate that blockade of the molecular programs enhancing macrophage recruitment or protumor bioactivity in tumors may represent tractable targets for anticancer therapy. Accordingly, genetic or pharmacologic blockade of CSF1 or its receptor has been reported to decrease macrophage presence in tissues and in some experimental solid tumors, correlating with diminished tumor angiogenesis, reduced primary tumor growth, and pulmonary metastasis (1, 2).

Experimental studies have recently revealed that B and T lymphocytes can exert protumor activity indirectly by regulating the bioactivity of myeloid cells, including macrophages, monocytes, and mast cells, resulting in resistance to endocrine therapies and development of metastasis (10-13). We reported that in the absence of a significant CD8<sup>+</sup> CTL response, CD4<sup>+</sup> T-effector lymphocytes potentiate mammary adenocarcinoma metastasis by directly enhancing the protumor bioactivity of TAMs (11). On the basis of these results, we hypothesized that human breast cancers containing leukocytic infiltrates dominated by CD4<sup>+</sup> T lymphocytes and CD68<sup>+</sup> macrophages, without significant CD8<sup>+</sup> T-cell infiltration, would have a higher relative risk for metastasis and therefore reduced overall survival (OS) of patients. In this article, we report on an immune signature consisting of CD68<sup>high</sup>/CD4<sup>high</sup>/CD8<sup>low</sup> that significantly correlates with reduced OS for patients with breast cancer. Moreover, to demonstrate the biologic significance of this signature, we investigated a combination of standard-of-care chemotherapy and agents that block TAM infiltration of mammary tumors in an aggressive transgenic mouse model of mammary adenocarcinoma development [MMTV-polyoma middle T (PyMT) mice; ref. 14], in which late-stage carcinogenesis and

pulmonary metastasis are regulated by CSF1 and tissue macrophages (15). We found that when TAM presence in mammary adenocarcinomas was minimized, antitumor immunity and CD8<sup>+</sup> CTL infiltration were enhanced; together, this improved chemosensitivity and resulted in reduced primary tumor development, significant decrease in pulmonary metastases, and improved OS, when compared with treatment using standard chemotherapy alone.

## RESULTS

### Single Immune Marker Analysis of Leukocyte Infiltration Predicts Breast Cancer Survival

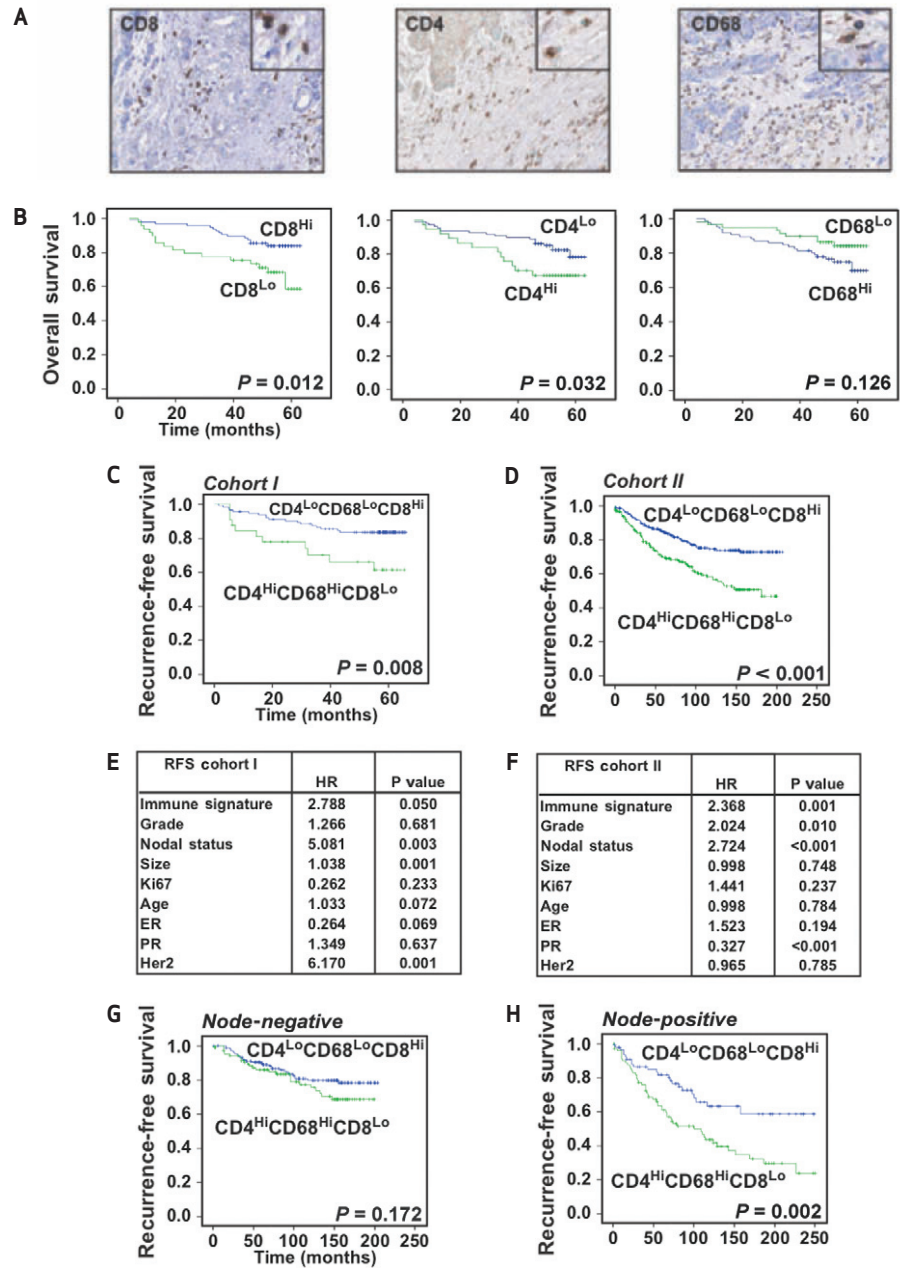
In previous studies, we demonstrated that in the absence of a significant CD8<sup>+</sup> CTL response, CD4<sup>+</sup> T lymphocytes indirectly promoted invasion and metastasis of mammary adenocarcinomas by directly regulating the protumor bioactivities of TAMs (11). From these data, we predicted that infiltration of primary human breast cancer by CD4<sup>+</sup> and CD8<sup>+</sup> T lymphocytes and CD68<sup>+</sup> macrophages would correlate with aspects of breast cancer regulating OS. To address this issue, we analyzed CD4<sup>+</sup>, CD8<sup>+</sup>, and CD68<sup>+</sup> leukocyte density in tissue microarrays consisting of tumor tissue obtained at the time of primary surgery from 179 treatment-naïve breast cancer patients (Fig. 1A). We employed a fully automated nuclear algorithm to quantify CD4<sup>+</sup>, CD8<sup>+</sup>, and CD68<sup>+</sup> cells following immunohistochemical (IHC) detection. For survival analyses, high and low thresholds for each marker were established using a classification and regression decision tree analysis with 10-fold cross-validation (16). Kaplan-Meier analyses indicated that, as single variables, "high" CD4<sup>+</sup> T-cell density ( $P = 0.032$ ) and "low" CD8<sup>+</sup> T-cell density ( $P = 0.012$ ) correlated with reduced OS, whereas CD68<sup>+</sup> cell density alone showed no statistical significance (Fig. 1B). However, analysis of CD68<sup>+</sup> and CD8<sup>+</sup> immune cell infiltration demonstrated an inverse association between stromal infiltration by CD68<sup>+</sup> macrophages and CD8<sup>+</sup> T lymphocytes in human breast cancer tissues (Spearman's rho,  $-0.38$ ;  $P < 0.001$ ; Supplementary Table S1).

### Three-Marker Immune Signature Is Prognostic for Breast Cancer Survival

Heterotypic interactions between diverse leukocyte populations often determine the outcome of immune responses in tissues (17). As such, we proposed that combined analysis of CD4, CD8, and CD68 would allow for improved prognostic stratification of breast cancer patients by assessing both antitumor immunity (i.e., CD8<sup>+</sup> density) and protumor immunity (i.e., high CD4<sup>+</sup> and CD68<sup>+</sup> leukocyte density). Thus, we predicted that an immune profile characterized by CD68<sup>low</sup>/CD4<sup>low</sup>/CD8<sup>high</sup> would represent primary breast cancer controlled by local resection, with improved OS and relapse-free survival (RFS). In contrast, an immune response characterized by CD68<sup>high</sup>/CD4<sup>high</sup>/CD8<sup>low</sup> would instead represent a population of patients at risk for distant metastasis and thus reduced OS. A classification and regression tree algorithm was used to define the signature in the screening cohort (Cohort I,  $n = 179$ ; Supplementary Fig. S1). High and low thresholds for each marker were established by decision tree analysis with 10-fold cross-validation

**Figure 1.** CD68/CD4/CD8 immune signature is an independent prognostic indicator of breast cancer survival.

**A**, high-magnification images (40×; 80× for inlays) of human breast cancer tissue sections showing immunoreactivity for representative CD68<sup>+</sup>, CD4<sup>+</sup>, and CD8<sup>+</sup> leukocyte infiltration. **B**, automated analysis of CD68<sup>+</sup>, CD4<sup>+</sup>, and CD8<sup>+</sup> immune cell detection, revealing relationship between leukocyte density and OS. Kaplan-Meier estimate of OS comparing autosome leukocyte high- and low-infiltration groups is shown; 179 samples from Cohort I were used for analyses, and log-rank (Mantel-Cox) *P* values are denoted for difference in OS. **C** and **D**, Kaplan-Meier estimate of RFS, comparing CD68<sup>high</sup>/CD4<sup>high</sup>/CD8<sup>low</sup> and CD68<sup>low</sup>/CD4<sup>low</sup>/CD8<sup>high</sup> immune profiles as assigned by random forest clustering to identify optimal thresholds using Cohort I (**C**). Identified CD68<sup>high</sup>/CD4<sup>high</sup>/CD8<sup>low</sup> and CD68<sup>low</sup>/CD4<sup>low</sup>/CD8<sup>high</sup> immune profiles were used to stratify a second independent cohort, Cohort II (**D**). Cohort I (*n* = 179) and Cohort II (*n* = 498) samples were assessed, and the log-rank (Mantel-Cox) *P* value is denoted for difference in RFS. **E** and **F**, results from multivariate Cox regression analysis of RFS for the CD68/CD4/CD8 signature in Cohort I (**E**) and Cohort II (**F**). Hazard ratios (HR) and *P* values are shown for all characteristics. **G** and **H**, RFS in node-positive breast cancer predicted by CD68/CD4/CD8 immune signature. Kaplan-Meier estimates of RFS comparing CD68<sup>high</sup>/CD4<sup>high</sup>/CD8<sup>low</sup> and CD68<sup>low</sup>/CD4<sup>low</sup>/CD8<sup>high</sup> immune profiles as assigned by random forest clustering of breast cancer tissues. breast cancers were stratified into node-negative (**G**) and node-positive (**H**) patients and analyzed for RFS. The log-rank (Mantel-Cox) *P* value is denoted for difference in RFS.



of each tree model (16). All patients were categorized as having either a CD68<sup>high</sup>/CD4<sup>high</sup>/CD8<sup>low</sup> or a CD68<sup>low</sup>/CD4<sup>low</sup>/CD8<sup>high</sup> immune signature, and the same thresholds were then applied to a validation cohort (Cohort II, *n* = 498 patients, primary tumor samples). Kaplan-Meier analysis in the 2 independent cohorts (totaling 677 patients) showed significantly reduced OS and RFS in patients whose tumors harbored the CD68<sup>high</sup>/CD4<sup>high</sup>/CD8<sup>low</sup> signature (Fig. 1C and D; Supplementary Fig. S2A and B). Multivariate Cox regression analysis revealed that the CD68<sup>high</sup>/CD4<sup>high</sup>/CD8<sup>low</sup> signature was an independent predictor of decreased OS and RFS after controlling for grade, nodal status, tumor size, estrogen receptor (ER), progesterone receptor (PR), HER2, and Ki-67 status in both cohorts (Fig. 1E and F; Supplementary Tables S2–S5), indicating that the immune signature predicted OS independently of established histopathologic parameters.

### Three-Marker Immune Signature Is an Independent Predictor of RFS in Node-Positive Patients

The OS of breast cancer patients is greatly reduced if metastasis to regional or draining lymph nodes is present at the time of primary tumor detection. Therefore, node-positive patients require aggressive treatment with neoadjuvant or adjuvant systemic chemotherapy, or targeted therapies such as anti-estrogens or trastuzumab. To assess whether immune infiltration by macrophages and T lymphocytes affected the survival of this high-risk group, we examined the impact of the CD68/CD4/CD8 signature following stratification for nodal status. Whereas the CD68/CD4/CD8 signature was not predictive in node-negative patients (Fig. 1G), Kaplan-Meier analysis of Cohort II demonstrated significantly reduced RFS in node-positive patients whose tumors harbored the CD68<sup>high</sup>/CD4<sup>high</sup>/CD8<sup>low</sup> immune signature

(Fig. 1H). Multivariate Cox regression analysis revealed that the CD68<sup>high</sup>/CD4<sup>high</sup>/CD8<sup>low</sup> signature was an independent predictor of decreased RFS after controlling for grade, tumor size, ER, PR, HER2, and Ki-67 status (Supplementary Table S6), indicating that the immune signature predicts RFS independently of established histopathologic parameters. Thus, tumor infiltration by macrophages and T lymphocytes may influence breast cancer recurrence in lymph node-positive patients, a group often aggressively treated with neoadjuvant and adjuvant chemotherapy.

### Cytotoxic Therapies Induce TAM Recruitment and CSF1 and IL-34 Cytokine Expression

These findings led us to hypothesize that blocking TAM infiltration in breast cancer patients bearing the CD68<sup>high</sup>/CD4<sup>high</sup>/CD8<sup>low</sup> signature might enhance antitumor T-cell responses and facilitate CD8<sup>+</sup> CTL infiltration and/or repolarization of CD4<sup>+</sup> T-cell responses toward T-helper 1 cell (T<sub>H</sub>1). Consistent with this hypothesis, we found an inverse association between stromal infiltration by CD68<sup>+</sup> macrophages and CD8<sup>+</sup> T lymphocytes in human breast cancer tissues (Spearman's rho, -0.38;  $P < 0.001$ ; Supplementary Table S1). On the basis of this observation, we postulated that chemosensitivity might in part be regulated by TAM and/or CD8<sup>+</sup> T-cell presence in breast cancer tissue. To address this, we initially evaluated leukocyte infiltration in a small cohort of freshly isolated breast tumors from women who had received neoadjuvant chemotherapy, compared with those undergoing primary surgery without preoperative treatment (Supplementary Table S7). We found a higher percentage of CD45<sup>+</sup>CD11b<sup>+</sup>CD14<sup>+</sup> macrophages in breast cancer from women who had received neoadjuvant chemotherapy than in tumors from women treated with surgery alone (Fig. 2A). In contrast, we observed no difference in tumor-infiltrating CD45<sup>+</sup>CD3<sup>+</sup>CD8<sup>+</sup> T lymphocytes between the 2 groups (Supplementary Fig. S3A).

To determine whether TAM presence in breast cancers was directly enhanced by chemotherapy, we evaluated leukocyte responses in MMTV-PyMT mice, a transgenic mouse model of mammary carcinogenesis, following treatment with paclitaxel (PTX; Supplementary Fig. S4). We found that infiltration of mammary tumors by CD45<sup>+</sup>CD11b<sup>+</sup>Ly6C<sup>low</sup>Ly6G<sup>-</sup>F4/80<sup>+</sup> TAMs was significantly increased following PTX treatment, with no significant change in the presence of CD3<sup>+</sup>CD8<sup>+</sup> T lymphocytes (Fig. 2B; Supplementary Fig. S3B). Similar PTX-induced TAM recruitment was observed in syngeneic orthotopic PyMT-derived tumors (Supplementary Fig. S3C). Consistent with our hypothesis, PTX treatment of MMTV-PyMT mice only modestly slowed primary tumor growth (Fig. 2B). For studies herein, we defined TAMs as CD45<sup>+</sup>CD11b<sup>+</sup>Ly6G<sup>-</sup>Ly6C<sup>low</sup>F4/80<sup>+</sup>, monocytic immature myeloid cells (iMC) as CD45<sup>+</sup>CD11b<sup>+</sup>Ly6G<sup>-</sup>Ly6C<sup>high</sup>, and granulocytic iMCs/neutrophils as CD45<sup>+</sup>CD11b<sup>+</sup>Ly6G<sup>high</sup>Ly6C<sup>+</sup> (Supplementary Fig. S5A and B), in agreement with previously published studies (18, 19).

To reveal molecular mediators involved in regulating PTX-induced TAM recruitment, we examined mRNA expression of several monocyte/macrophage cytokines and chemokines in murine mammary epithelial carcinoma cells (MEC) following exposure to several forms of cytotoxic therapy *in vitro*. *CSF1*, *CCL8/MCP2*, and *IL34* mRNAs were increased in MMTV-PyMT-derived MECs following exposure to PTX

(Fig. 2C). Of these, *CSF1* and *IL34* mRNAs were also increased following exposure to either CDDP or ionizing radiation (Fig. 2D; Supplementary Fig. S3D). Increased mRNA expression was not merely a response of malignant PyMT-derived MECs (pMEC), because a similar induction was also observed in nontransgenic MECs exposed to PTX in culture (Fig. S3E). Similarly, *CSF1* mRNA expression was also induced by PTX and CDDP in 5 of 6 human breast cancer cell lines reflecting the major subtypes of breast cancer (Fig. 2E). *In vivo*, *CSF1* mRNA was increased in mammary tissue of MMTV-PyMT mice following treatment with either PTX or ionizing radiation (Fig. 2F; Supplementary Fig. S3F). Together, these data indicate that induction of *CSF1* (and *IL34*) mRNA and subsequent TAM recruitment into mammary tissue represent a common response of MECs to cytotoxic agents.

### Blockade of Chemotherapy-Induced TAM Recruitment

To determine whether tumor-infiltrating TAMs also regulate sensitivity of MECs to cytotoxic therapy, we blocked TAM infiltration *in vivo* with immunologic and pharmacologic agents (Supplementary Fig. S4) and evaluated myeloid cell infiltration of tumors from treated mice (Supplementary Fig. S5). Mice bearing orthotopic mammary tumors were treated with neutralizing monoclonal antibodies (mAb) CSF1 (clone 5S1) or CD11b (clone M1/70), or a competitive ATP inhibitor with potent (nM) specificity for CSF1 and cKIT receptor tyrosine kinases (PLX3397), either as a monotherapy or in combination with PTX. CD11b is an integrin cell adhesion molecule expressed on granulocytes, macrophages, monocytes, dendritic cells (DC), and natural killer cells that in part regulates transendothelial migration of cells into tissue and tumor parenchyma. PLX3397 has 10- to 100-fold selectivity for cKIT and CSF1R, as opposed to other related kinases, such as KDR (see Supplementary Fig. S6A and Methods; ref. 20).

Fluorescence-activated cell sorting analysis of the predominant myeloid subtypes infiltrating mammary tumors revealed that either as monotherapy, or in combination with PTX, CD45<sup>+</sup>CD11b<sup>+</sup>Ly6C<sup>-</sup>Ly6G<sup>-</sup>F4/80<sup>+</sup> TAM recruitment was significantly diminished following treatment with either αCSF1 mAb or PLX3397, with no effect on infiltration of CD45<sup>+</sup>CD11b<sup>+</sup>Ly6G<sup>high</sup> iMCs or CD45<sup>+</sup>CD11b<sup>low</sup>/Ly6C<sup>-</sup>CD22<sup>-</sup>Ly6G<sup>-</sup>CD11c<sup>high</sup>MHCII<sup>high</sup> DCs (Fig. 3A and B; Supplementary Fig. S5A and B). Treatment with αCD11b mAb decreased both TAM and iMC infiltration (Fig. 3A). Analysis of the maturation and differentiation status of TAMs remaining in mammary tumor tissue following αCSF1 or PLX3397 treatment revealed no significant change in CD11b, CD11c, F4/80, CD45, or MHCII expression (Supplementary Fig. S5B). However, examination of mammary tumor sections revealed a population of perivascular CSF1-independent F4/80<sup>+</sup> TAMs remaining (Fig. 3C). Blockade of TAM recruitment was a direct effect of CSF1/CSF1R blockade: *In vitro* CSF1R inhibition efficiently blocked CD11b<sup>+</sup> monocyte chemotaxis in response to control or PTX-treated pMEC-conditioned medium, with no effect on chemotaxis of CD3<sup>+</sup> T lymphocytes (Fig. 3D; Supplementary Fig. S3G). These results were mirrored *in vivo*; treatment of late-stage MMTV-PyMT mice with PLX3397 significantly inhibited both steady-state and PTX-induced tumor infiltration by CD45<sup>+</sup>CD11b<sup>+</sup>Ly6C<sup>-</sup>Ly6G<sup>-</sup>F4/80<sup>+</sup> TAMs (Fig. 3E; Supplementary Fig. S5) without altering TAM maturation/differentiation (Supplementary Fig. S6B).

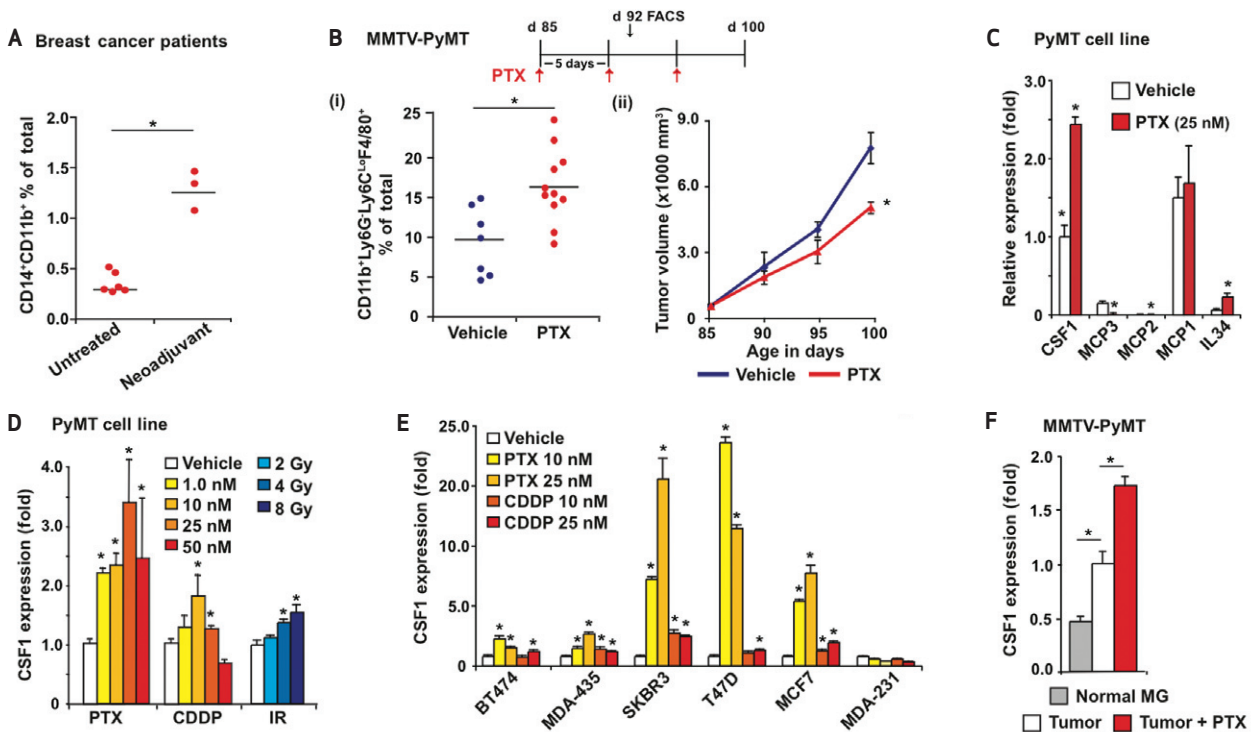


**Figure 2.** Cytotoxic therapy induces macrophage recruitment, as well as *CSF1* and *IL-34* mRNA expression. **A**, macrophage percentage in fresh human primary breast cancer tissues, depicted as mean of CD45<sup>+</sup>CD11b<sup>+</sup>CD14<sup>+</sup> macrophages as a percentage of total cells (analyzed by flow cytometry). “Neo-adjuvant” denotes patients who received chemotherapy prior to surgical resection of their primary breast cancer, as opposed to those who did not, denoted as “untreated”; \*, statistically significant differences ( $P = 0.004$ ) between the 2 groups. **B**, PTX-induced *CSF1* mRNA expression regulates tumor infiltration of macrophages and limits PTX response. (i), TAM percentage in mammary tumors of MMTV-PyMT mice following PTX treatment with mean number of CD45<sup>+</sup>Ly6G<sup>+</sup>Ly6C<sup>+</sup>CD11b<sup>+</sup>F4/80<sup>+</sup> TAMs as a percentage of total cells shown (analyzed by flow cytometry); (ii), primary tumor growth reduced by treatment with PTX. The 85-day-old MMTV-PyMT mice were treated with PTX and total tumor burden per animal was assessed every 5 days until endpoint. Treatment schematic is depicted at top, and data are displayed as mean tumor burden  $\pm$  SEM; \*, statistically significant differences between controls and PTX-treated mice ( $>8$  mice/group). **C**, expression of monocyte/macrophage chemoattractants following chemotherapy. Quantitative reverse transcriptase PCR (qRT-PCR) analyses of *CSF1*, *MCP1*, *MCP2*, *MCP3*, and *IL34* expression in MMTV-pMECs treated with PTX for 24 hours ex vivo, expressed as mean fold change, compared with controls. Samples were assayed in triplicate for each tested condition; \*, statistically significant differences between control and PTX-treated groups. **D**, Dose-dependent expression of *CSF1* following chemotherapy or radiation therapy. qRT-PCR analysis of mRNA expression in MMTV-PyMT-derived pMECs 24 hours after treatment with either cisplatin (CDDP), PTX, or a single dose of ionizing radiation, expressed as mean fold change, compared with control  $\pm$  SEM. Drug and radiation doses are shown. Samples were assayed in triplicate for each tested condition; \*, statistically significant differences between control and the indicated treatment. **E**, *CSF1* expression induced by chemotherapy in human breast carcinoma cell lines. qRT-PCR analysis of mRNA expression in BT474, MDA-MB-435, SKBR3, T47D, MCF7, and MDA-MB-231 at 24 hours after treatment with either CDDP or PTX, expressed as mean fold change, compared with vehicle-treated cells  $\pm$  SEM. Chemotherapeutic doses are denoted. Samples were assayed in triplicate for each condition; \*, statistically significant differences between control and indicated treatment. **F**, *CSF1* expression induced by cytotoxic therapy in MMTV-PyMT mammary tumors. qRT-PCR analysis of mRNA expression isolated from normal mammary tissue or MMTV-PyMT mammary tumors from mice treated with either PTX (10 mg/kg) every 5 days, or ionizing radiation (single dose of 8 Gy), expressed as mean fold change, compared with vehicle-treated tumors (4 mice/group). SE is depicted; \*, statistically significant differences ( $P < 0.05$ , Mann-Whitney) for all gene expression analyses (**C-F**).

We next treated 80-day-old MMTV-PyMT mice, or mice bearing syngeneic orthotopic PyMT-derived tumors ( $\sim 1.0$  cm) with  $\alpha$ CSF1,  $\alpha$ CD11b, or PLX3397 (vs controls) for 5 days, followed by 4 cycles of PTX (10 mg/kg, i.v.; Supplementary Fig. S4). Primary tumor burden at study endpoints (2.0 cm primary tumors or 100 days of age) was significantly reduced in mice treated with combined  $\alpha$ CSF1/PTX,  $\alpha$ CD11b/PTX, or PLX3397/PTX therapy, compared to mice treated with these as single agents (Fig. 4A and B; Supplementary Fig. S7A). Similar results were observed in syngeneic mice bearing orthotopic PyMT-derived mammary tumors receiving combined PLX3397/carboplatin (CBDCA) therapy (Fig. 4B).

Mammary tumors in MMTV-PyMT mice progress through well-defined stages of cancer development, similar to progression of breast cancer in women, including tissue with florid ductal hyperplasia, ductal carcinoma *in situ* with early stromal invasion, and poorly differentiated invasive ductal carcinoma (15, 21). Using this staging criterion, we observed that mammary

tumors arising in MMTV-PyMT mice treated with combined PLX3397/PTX therapy exhibited decreased development of late-stage carcinoma, compared with tumors in age-matched mice treated with either PTX or PLX3397 as monotherapy (Fig. 4C; Supplementary Fig. S7B). Moreover, the late-stage carcinomas that did develop in PLX3397/PTX-treated mice contained large areas of necrosis (Supplementary Fig. S7C) characterized by increased presence of apoptotic cells, as measured by cleaved caspase 3-positivity (Fig. 4D) with no accompanying change in epithelial proliferation (Supplementary Fig. S7D).

### Decreased Vascular Density Accompanies Improved Chemosensitivity

It is known that TAMs provide VEGF to developing mammary tumors and thereby regulate angiogenic programming of tissue (22–24). Chemosensitivity to CDDP in MMTV-PyMT mice is in part regulated by myeloid-derived VEGF (25); thus, we sought to determine if TAM depletion altered VEGF expression and/

or density of CD31<sup>+</sup> vessels in MMTV-PyMT mice treated with PTX. Whereas total *VEGF* mRNA expression was significantly reduced by PLX3397 (Fig. 4E), this 70% reduction did not correlate with a change in vascular density (Fig. 4F). In contrast, combined PLX3397/PTX therapy resulted in a significant reduction in CD31<sup>+</sup> vessel density within mammary tumors, paralleling induction of apoptosis and necrosis (Fig. 4F).

### CSF1-Signaling Blockade Enhances Antitumor Immunity and CTL Infiltration in Response to Chemotherapy

Because analysis of human breast cancer tissues revealed that high stromal TAM density inversely correlated with CD8<sup>+</sup> T-cell

infiltration (Supplementary Table S1), we predicted that depletion of TAMs would enhance CD8<sup>+</sup> CTL infiltration and thereby foster an antitumor immune microenvironment. Analyses of tumor-infiltrating T lymphocytes in mice treated with  $\alpha$ CSF1/PTX or PLX3397/PTX by flow cytometry or IHC revealed significantly increased presence of CD4<sup>+</sup> and CD8<sup>+</sup> T cells in mammary tumors (Fig. 5A and B; Supplementary Fig. S8A). Consistent with these findings, cytokine mRNA expression in mammary tissue derived from PLX3397/PTX-treated MMTV-PyMT mice revealed increased mRNA expression of cytotoxic effector molecules, including *IFN- $\gamma$* , *granzyme A*, *granzyme B*, *perforin-1*, and the type 1 DC effector molecules *IL12p35* and *IFN- $\alpha$*  (Fig. 5C). In contrast, expression of the immunosuppressive molecule *arginase-1* was

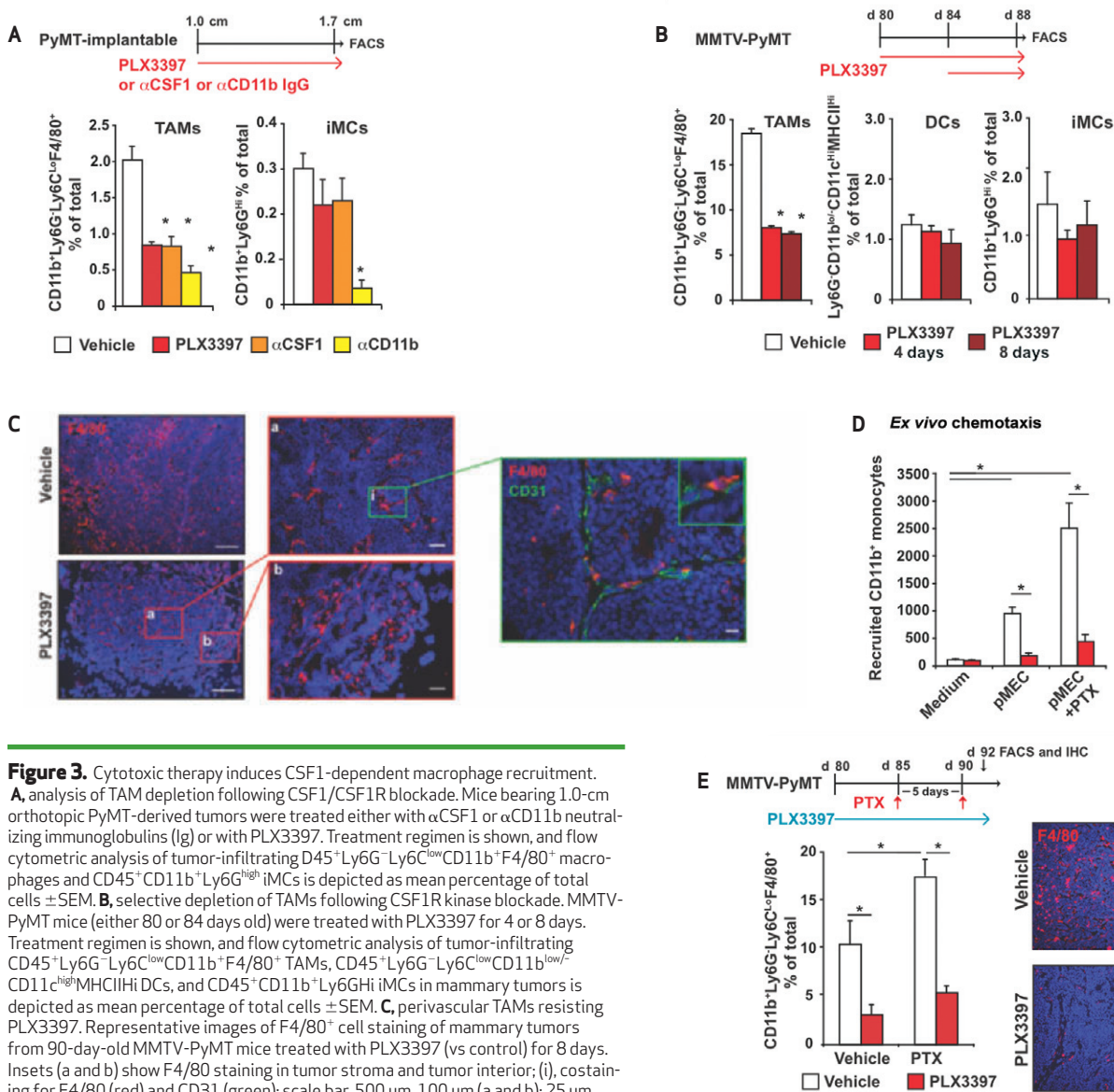


**Figure 3.** Cytotoxic therapy induces CSF1-dependent macrophage recruitment. **A**, analysis of TAM depletion following CSF1/CSF1R blockade. Mice bearing 1.0-cm or thoptopic PyMT-derived tumors were treated either with  $\alpha$ CSF1 or  $\alpha$ CD11b neutralizing immunoglobulins (Ig) or with PLX3397. Treatment regimen is shown, and flow cytometric analysis of tumor-infiltrating CD45<sup>+</sup>Ly6G<sup>-</sup>Ly6C<sup>low</sup>CD11b<sup>+</sup>F4/80<sup>+</sup> macrophages and CD45<sup>+</sup>CD11b<sup>+</sup>Ly6G<sup>high</sup>iMCS is depicted as mean percentage of total cells  $\pm$  SEM. **B**, selective depletion of TAMs following CSF1R kinase blockade. MMTV-PyMT mice (either 80 or 84 days old) were treated with PLX3397 for 4 or 8 days. Treatment regimen is shown, and flow cytometric analysis of tumor-infiltrating CD45<sup>+</sup>Ly6G<sup>-</sup>Ly6C<sup>low</sup>CD11b<sup>+</sup>F4/80<sup>+</sup> TAMs, CD45<sup>+</sup>Ly6G<sup>-</sup>Ly6C<sup>low</sup>CD11b<sup>low</sup>/CD11c<sup>high</sup>MHCII<sup>hi</sup>DCs, and CD45<sup>+</sup>CD11b<sup>+</sup>Ly6G<sup>hi</sup>iMCS in mammary tumors is depicted as mean percentage of total cells  $\pm$  SEM. **C**, perivascular TAMs resisting PLX3397. Representative images of F4/80<sup>+</sup> cell staining of mammary tumors from 90-day-old MMTV-PyMT mice treated with PLX3397 (vs control) for 8 days. Insets (a and b) show F4/80 staining in tumor stroma and tumor interior; (i), costaining for F4/80 (red) and CD31 (green); scale bar, 500  $\mu$ m, 100  $\mu$ m (a and b); 25  $\mu$ m (i). **D**, peripheral blood lymphocyte (PBL) migration in response to conditioned medium from MMTV-PyMT MECs treated with either vehicle or PTX (25 nM for 24 hours), evaluated by Boyden chamber assay. CD45<sup>+</sup>CD11b<sup>+</sup> peripheral blood monocytes after migration to the lower chamber, in the presence or absence of PLX3397 (50 nM), as quantified by flow cytometry. Data are depicted as mean cell number assayed in triplicate. **E**, PTX-induced TAM recruitment inhibited by PLX3397. TAM density in mammary tumors removed from MMTV-PyMT mice following treatment with PTX  $\pm$  PLX3397. Treatment regimen is shown with mouse age, and data are depicted as mean number of CD45<sup>+</sup>Ly6G<sup>-</sup>Ly6C<sup>low</sup>CD11b<sup>+</sup>F4/80<sup>+</sup> cells as a percentage of total cells  $\pm$  SEM (analyzed by flow cytometry, >5 mice/group). Representative IHC staining for F4/80 (red) and nuclear DNA (blue) from the same cohort of animals is shown. Scale bar, 500  $\mu$ m; \*, statistically significant differences ( $P < 0.05$ , Mann-Whitney) in **A–E**.

decreased by PLX3397/PTX therapy (Fig. 5C). This reprogramming of the immune microenvironment was accompanied by increased tumor infiltration of CD45<sup>+</sup>CD11b<sup>low/-</sup>CD19<sup>-</sup>Ly6G<sup>-</sup>Ly6C<sup>low</sup>CD11c<sup>high</sup>MHCII<sup>high</sup> DCs (Fig. 5D), indicating that combined treatment of MMTV-PyMT mice with PLX3397/PTX fostered an antitumor immune response by T lymphocytes expressing high levels of cytotoxic effector molecules.

Given these findings, we assessed the capacity of TAMs (isolated from mammary tumors of MMTV-PyMT mice) to directly repress CD8<sup>+</sup> T-cell activation *in vitro*. Using carboxyfluorescein succinimidyl ester (CFSE) dilution as a marker for T-cell proliferation, we found that CD45<sup>+</sup>CD11b<sup>+</sup>F4/80<sup>+</sup>Ly6G<sup>-</sup>Ly6C<sup>low</sup> TAMs significantly repressed CD8<sup>+</sup> T-cell activation and proliferation in a dose-dependent manner (Fig. 5E) that was reflective of the altered ratio of TAMs to CD8<sup>+</sup> T cells in mammary tumors of untreated versus PLX3397/PTX-treated MMTV-PyMT mice (Fig. 5F).

One mechanism by which TAMs may suppress CD8<sup>+</sup> T cells involves expression of inhibitory B7 family members that interact with “checkpoint” receptors expressed on infiltrating CD8

T cells. In particular, growing interest has been expressed in the PD1- PDL1 ligand system, in which PDL1/B7-H1 expression by TAMs represents a major source of the inhibitory PD1 ligand. Thus, we evaluated TAMs isolated from mammary tumors for expression of PDL1/B7-H1 and PDL2/B7-DC, as well as costimulatory molecules CD80 and CD86, and MHCII. TAMs expressed high levels of MHCII and B7-H1, but relatively lower levels of CD80 and CD86, indicating a possible role in inducing tolerance/anergy in tumor antigen-specific CD4<sup>+</sup> and CD8<sup>+</sup> T lymphocytes (Supplementary Fig. S5C).

## Macrophage Depletion Enhances Chemotherapeutic Response in a CD8<sup>+</sup> CTL-Dependent Manner

To determine whether increased chemosensitivity of mammary tumors in PLX3397/PTX-treated mice was dependent on enhanced CD8<sup>+</sup> T-cell response, we depleted CD8<sup>+</sup> T cells from late-stage MMTV-PyMT mice treated with PTX or PLX3397 or both. Findings from this study revealed that the improved outcome with enhanced chemosensitivity resulting

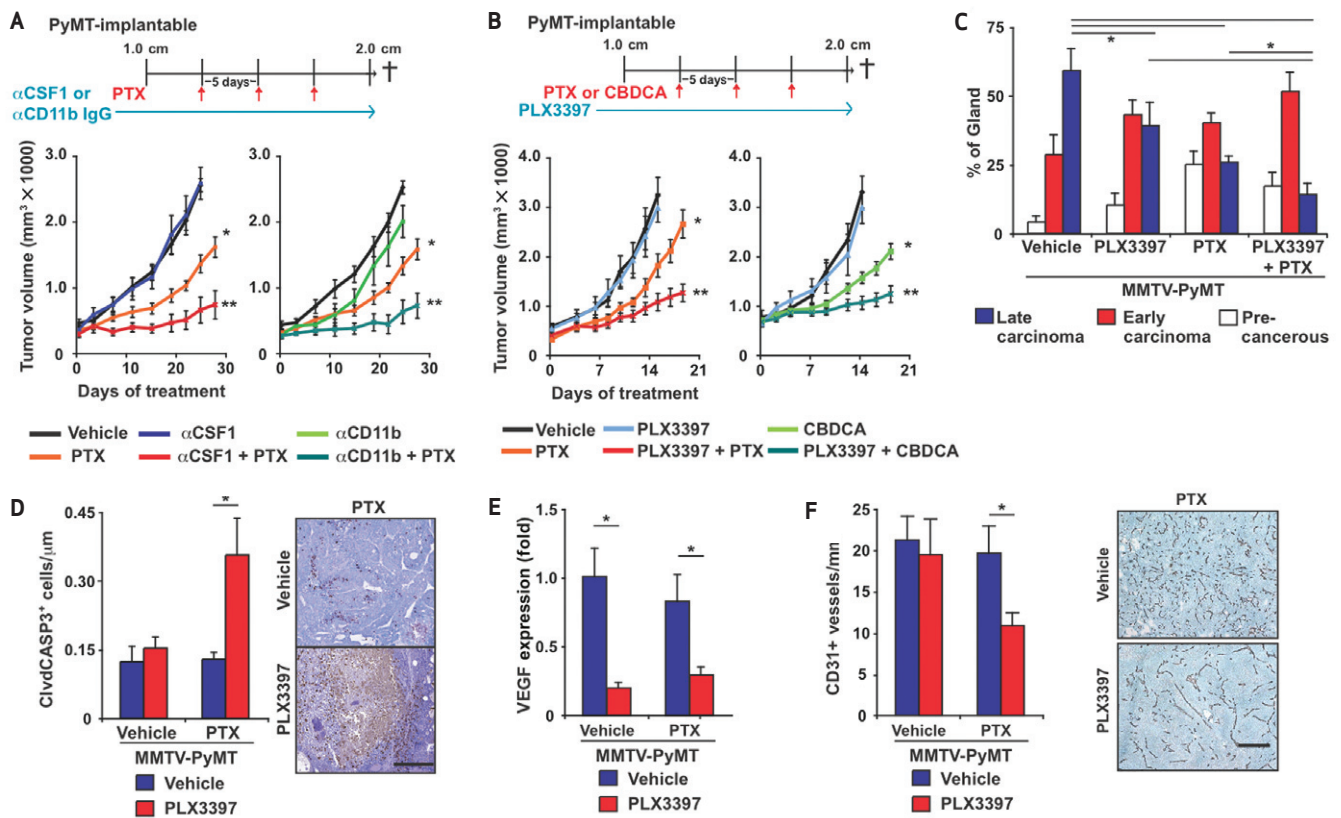
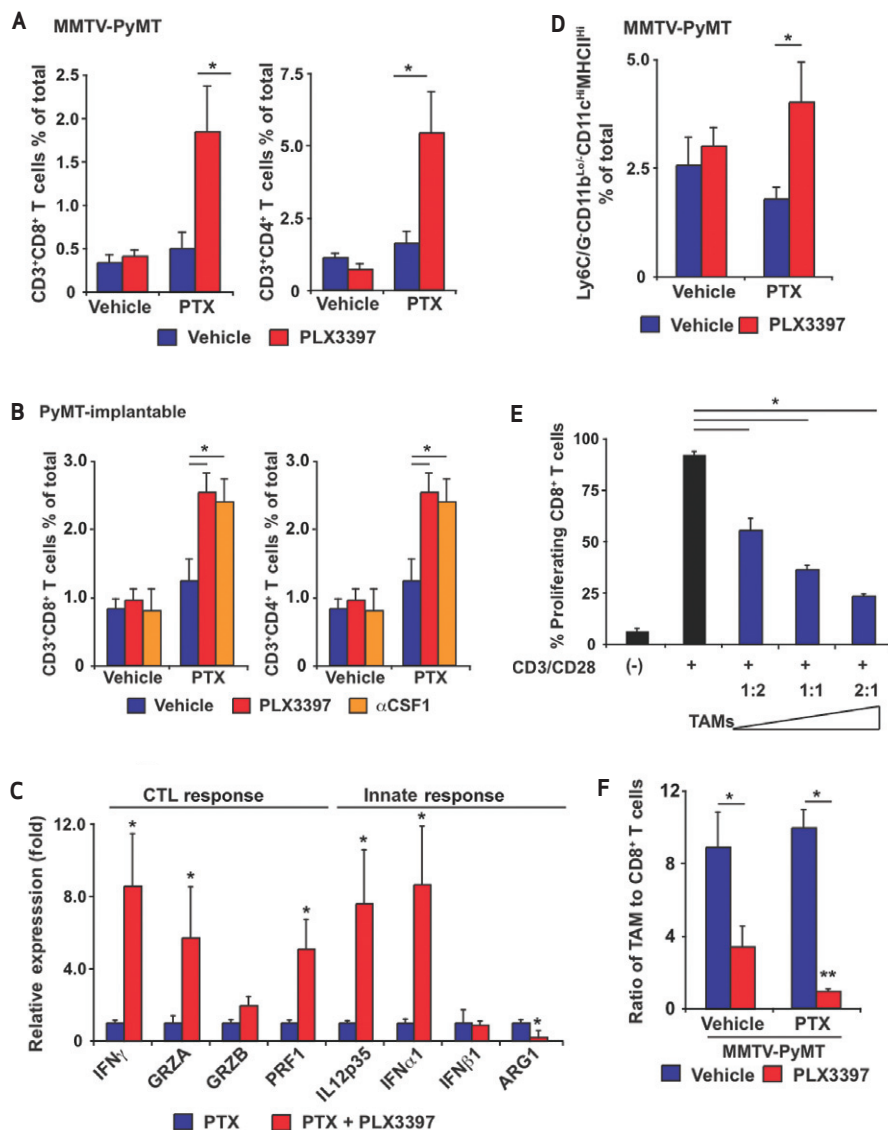


**Figure 4.** Macrophage depletion improves response to chemotherapy. **A** and **B**, primary tumor growth reduced by treatment with macrophage-depleting agents in combination with chemotherapy. Orthotopic PyMT-derived tumors were grown to a median diameter of 1.0 cm, and mice were then treated with PTX, CBDCA, and/or αCSF1, αCD11b neutralizing Igs ± PLX3397 for 21 or 28 days, with total tumor burden per animal assessed every 2 to 3 days. Treatment regimens are depicted for all cohorts, and data displayed as mean tumor burden ± SEM; \*, statistically significant differences between vehicle- and PTX-treated mice. \*\*, significant differences between mice treated with PTX alone and mice treated with PTX/PLX3397 or αCSF1 or αCD11b in combination. **C**, histologic stage analysis of MMTV-PyMT tumors. Tumors from 100-day-old MMTV-PyMT mice treated with PTX or PLX3397 or both were assessed for the presence of premalignant tissue and early- and late-stage carcinoma; data expressed as mean percentage of total gland area ± SEM. **D**, quantification of cleaved caspase-3-positive cells in mammary tumors of MMTV-PyMT mice treated with PTX or PLX3397 or both versus control (vehicle). Graph depicts mean positive cells per μm<sup>2</sup> of tumor tissue. Representative images show cleaved caspase-3-positive cells (brown staining) in tumors of MMTV-PyMT mice treated with vehicle or PTX or PLX3397 or both; scale bar, 500 μm. **E**, VEGF mRNA expression assessed by qRT-PCR of tumor tissue from MMTV-PyMT mice treated with vehicle or PTX or PLX3397 or both. Graph depicts mean fold change in gene expression compared with vehicle-treated control group. **F**, quantification of CD31<sup>+</sup> positive vessels in mammary tumors from MMTV-PyMT mice treated with PTX or PLX3397 or both, versus control (vehicle). Data represent the mean number of CD31<sup>+</sup> positive vessels per mm<sup>2</sup> of carcinoma tissue. Representative photomicrographs show CD31<sup>+</sup> positive vessels (brown staining); scale bar, 400 μm; \*, statistically significant differences ( $P < 0.05$ , Mann-Whitney) in **C-F**.

**Figure 5.** PTX in combination with PLX397 induces antitumor T-cell response. **A** and **B**, tumor infiltration by T lymphocytes enhanced by combined PTX and CSF1 or CSF1R blockade. Flow cytometric analyses of tumor infiltrating CD3<sup>+</sup>CD8<sup>+</sup> and CD3<sup>+</sup>CD4<sup>+</sup> T lymphocytes depicted as the mean number of positive cells, assessed as a percentage of total cells following treatment of MMTV-PyMT mice with PTX or PLX3397 or both (**A**), or treatment of mice having orthotopic PyMT-derived tumors with combined PTX/ $\alpha$ CSF1 or PTX/PLX3397 (**B**), compared with controls. Mean values  $\pm$ SEM are depicted. **C**, cytokine mRNA expression assessed in orthotopic PyMT-derived tumors from mice treated with PTX alone or in combination with PLX3397. Graph depicts mean fold change in mRNA expression compared with PTX treatment group (5 animals/group). SEM is depicted. **D**, tumor infiltration by DCs enhanced by combined PTX/PLX3397. Flow cytometric analysis of tumor-infiltrating CD45<sup>+</sup>Ly6G<sup>-</sup>Ly6C<sup>low</sup>CD11b<sup>low</sup>-CD11c<sup>high</sup>MHCII<sup>high</sup> DCs depicted as mean percentage of positive cells as a percentage of total cells from MMTV-PyMT mice treated with PTX or PLX3397 or both, versus controls. **E**, CD8<sup>+</sup> T-lymphocyte activation repressed by TAMs. Purified T cells were loaded with CFSE and activated *in vitro* by plate-bound CD3/28 and cocultured with the indicated ratio of CD45<sup>+</sup>Ly6G<sup>-</sup>Ly6C<sup>low</sup>CD11b<sup>+</sup>F4/80<sup>+</sup> TAMs isolated from late-stage mammary tumors of MMTV-PyMT mice. Data are depicted as the percentage of live CD8<sup>+</sup> T lymphocytes exhibiting CFSE dilution after 60 hours. Data are representative of 2 independent experiments run in triplicate. Error bars represent SEM. **F**, analysis of the ratio of tumor-infiltrating CD45<sup>+</sup>Ly6G<sup>-</sup>Ly6C<sup>low</sup>CD11b<sup>+</sup>F4/80<sup>+</sup> TAMs to CD3<sup>+</sup>CD8<sup>+</sup> T lymphocytes depicted as mean ratio (TAM/CD8 CTL)  $\pm$  SEM from MMTV-PyMT mice treated with vehicle or with PTX and/or PLX3397. \*, statistically significant differences ( $P < 0.05$ , Mann-Whitney) in **A-F**. \*\*, statistically significant differences ( $P < 0.05$ , Mann-Whitney) between PLX3397-treated groups in **F**.



from combined PLX3397/PTX therapy was indeed a CD8<sup>+</sup> T-cell-dependent response (Fig. 6A and B; Supplementary Fig. S8B). We found that CD8 depletion also resulted in increased tumor grade and decreased presence of cleaved caspase-3-positive cells in mice that had received combined PLX3397/PTX therapy (Fig. 6C and D). Taken together, these data indicate that the enhanced cytotoxic response elicited by CSF1R-signaling blockade was CD8<sup>+</sup> T-cell-dependent.

### Combined Macrophage Depletion and Chemotherapy Blocks Metastasis in a CD8-Dependent Manner

Long-term survival of breast cancer patients is often limited by disseminated metastases following surgical resection of primary tumors. Analysis of leukocyte profiles in human breast cancers demonstrated that OS, and thus presumably metastatic spread, were regulated by the spectrum of tumor-infiltrating T lymphocytes and macrophages present. In MMTV-PyMT mice, although neither CSF1R-signaling blockade nor PTX therapy alone inhibited development of pulmonary metastasis, mice receiving combined PLX3397/PTX exhibited >85% reduction in

pulmonary metastases that was in part CD8<sup>+</sup> T-cell-dependent (Fig. 6E).

### Macrophages and CD8 Infiltration Predicts Survival and Chemotherapeutic Response

Overall, our data indicated that in the absence of TAMs, antitumor CD8<sup>+</sup> CTLs bolster response to chemotherapy and thereby influence outcome; thus, we predicted that TAM and CD8 T-cell ratios would correlate with pathologic responses in patients with breast cancer. Accordingly, we analyzed *CD68* and *CD8a* mRNA expression in a cohort of 311 patients constructed from 2 independent datasets (26, 27). All patients provided fine-needle aspirates (FNA) prior to neoadjuvant chemotherapy, and pathologic response was assessed at the time of definitive surgery. *CD8* mRNA expression in FNA samples correlated with pathologic complete response (pCR;  $R = 0.216$ ;  $P < 0.001$ ); however, *CD68* did not. With median expression as a threshold, examination of both *CD8* and *CD68* mRNA revealed 3 groups—*CD68* > *CD8*, *CD68* < *CD8*, and *CD68* = *CD8* (denoted *CD68*<sup>high</sup>/*CD8*<sup>low</sup>, *CD68*<sup>low</sup>/*CD8*<sup>high</sup>, and *CD68*/*CD8*).

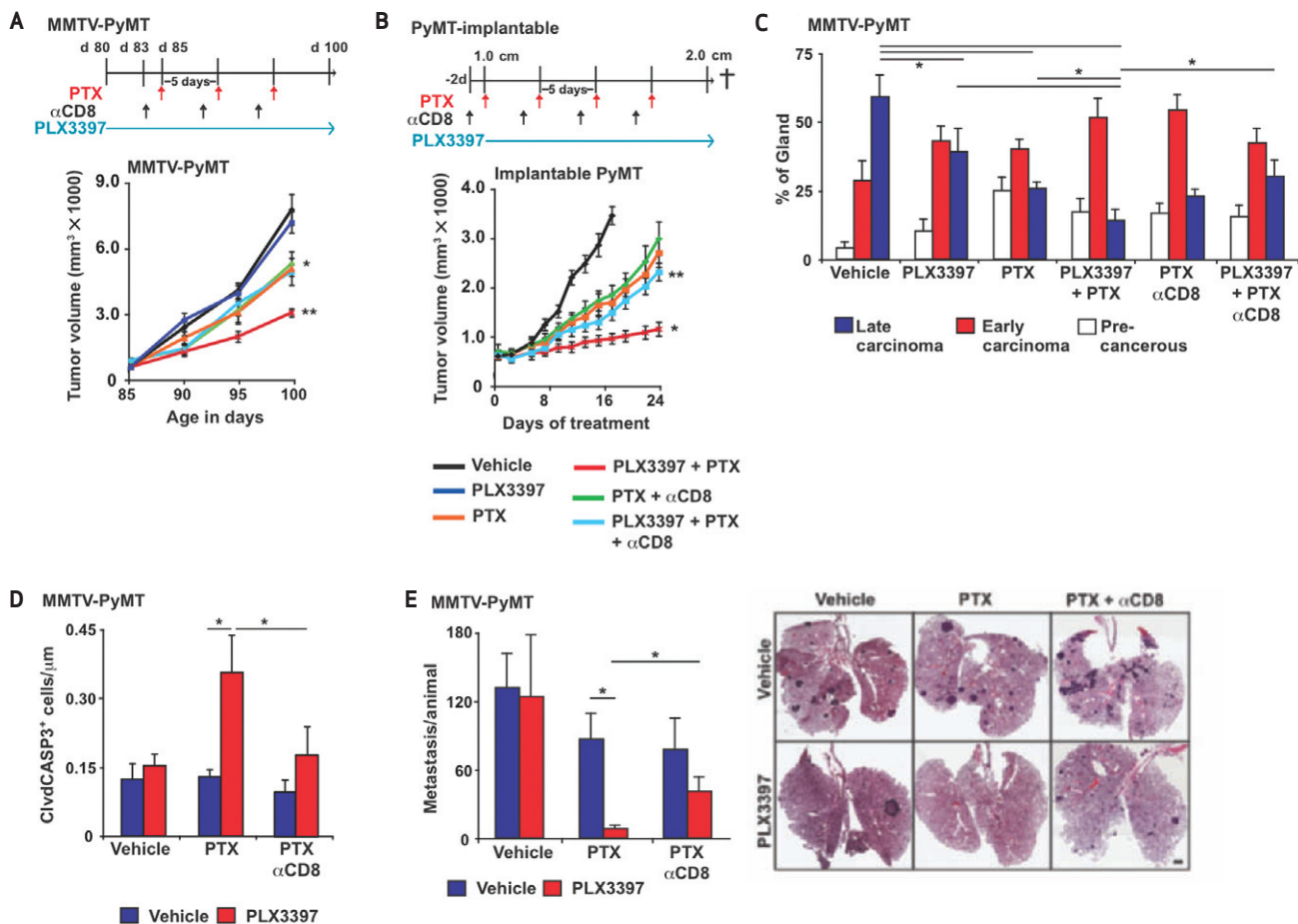


**Figure 6.** Combined PLX3397 and PTX treatment inhibits metastasis in a CD8-dependent manner. **A** and **B**, improved outcome following PLX3397/PTX treatment dependent on CD8<sup>+</sup> T cells. **A**, 85-day-old MMTV-PyMT mice were treated with PTX or PLX3397 or both, as well as anti-CD8 IgG. Total tumor burden per animal was assessed every 5 days. **B**, orthotopic PyMT-derived tumors were grown to a median diameter of 1.0 cm, at which time mice were treated with PTX or PLX3397 or both in combination with anti-CD8 or control IgG for 21 days, and total tumor burden per animal was assessed every 2 to 3 days. Treatment regimens are depicted along with SEM; \*, statistically significant differences between mice treated with PTX alone and those treated with PLX3397/PTX. \*\*, significant differences between mice treated with PLX3397/PTX and those treated with anti-CD8 and PTX/PLX3397/control IgG. **C**, histologic stage analysis of MMTV-PyMT tumors. Tumors from 100-day-old MMTV-PyMT mice treated with anti-CD8 IgG or with PTX and/or PLX3397 were assessed for presence of premalignant tissue and early- and late-stage carcinoma; data expressed as mean percentage of total gland area  $\pm$  SEM. **D**, quantification of cleaved caspase-3-positive cells in mammary tumors of MMTV-PyMT mice treated with anti-CD8 IgG or with PTX and/or PLX3397 versus control (vehicle). Graph depicts mean positive cells per  $\mu$ m<sup>2</sup> of tumor tissue. **E**, quantification of metastatic foci per lung section per mouse from 100-day-old MMTV-PyMT mice treated with PTX and/or PLX3397 and/or anti-CD8 IgG, versus controls. Each lung was serially sectioned, 6 sections 100  $\mu$ m apart were stained with hematoxylin and eosin (H&E), and the total number of metastatic foci (>8 cells) was quantified per mouse ( $n \geq 10$  mice per cohort). SEM is depicted. \*, Statistically significant differences ( $P < 0.05$ , Mann-Whitney). Representative photomicrographs of lung tissue sections reveal metastatic foci from 100-day-old MMTV-PyMT mice treated with vehicle or with PTX and/or PLX3397. Scale bar, 500  $\mu$ m.

CD8<sup>equal</sup>, respectively)—with the CD68<sup>high</sup>/CD8<sup>low</sup> group correlating with a significantly lower rate of pCR (7%) and the CD68<sup>low</sup>/CD8<sup>high</sup> exhibiting the highest rate of pCR at 27% (Fig. 7A). Thus, the ratio of CD68/CD8a expression represents a predictive response biomarker for neoadjuvant chemotherapy.

We next evaluated CD68 and CD8a mRNA expression in breast cancers representing ~4000 patients assembled from 22 retrospective gene expression datasets (Supplementary Table S8). Median expression for both CD8 and CD68 was used to determine high and low groups. All patients were categorized as either CD68<sup>high</sup>/CD8<sup>low</sup> or CD68<sup>low</sup>/CD8<sup>high</sup>. Kaplan-Meier estimates of survival demonstrated significantly reduced OS in the CD68<sup>high</sup>/CD8<sup>low</sup> group (Fig. 7B). Not surprisingly, these

gene expression results were validated using Kaplan-Meier analysis of OS on IHC data from Cohort I and II stratified for CD68<sup>high</sup>/CD8<sup>low</sup> or CD68<sup>low</sup>/CD8<sup>high</sup> (Supplementary Fig. S9A and B).

Because breast cancer represents a spectrum of distinct molecular subtypes (luminal A, luminal B, HER2-positive, basal type/triple negative), possessing distinct histopathologic and molecular features and correlating with differential responses to therapy and outcome (28–30), we evaluated CD68/CD8 expression within breast cancer subtypes. CD68<sup>high</sup>/CD8<sup>low</sup> expression correlated with reduced OS for breast cancer patients whose tumors were classified as either basal or HER2-positive (Fig. 7C; Supplementary Fig. S10).

## DISCUSSION

The immune microenvironment in which a tumor evolves influences multiple parameters of the tumorigenic process. In this article we demonstrate that the immune microenvironment in breast cancer is a predictor of RFS and OS. Moreover, we provide evidence that response to chemotherapy is in part regulated by the immune microenvironment and that cytotoxic therapies induce neoplastic cells to produce monocyte/macrophage recruitment factors, including CSF1 and IL-34, which in turn enhance CSF1R-dependent macrophage infiltration into mammary adenocarcinomas. This is significant in light of our finding that blockade of the CSF1-signaling pathway mediating TAM recruitment, in combination with chemotherapy, decreases primary tumor progression, reduces metastasis, and improves survival—a CD8<sup>+</sup> T-cell-dependent outcome resulting from a reprogrammed immune microenvironment that fosters antitumor immunity. These data provide a compelling rationale for combinatorial therapies targeting TAM recruitment, notably CSF1R-mediated signaling pathways, in combination with cytotoxic therapy for breast cancer.

## The Immune Microenvironment in Breast Cancer Predicts Outcome

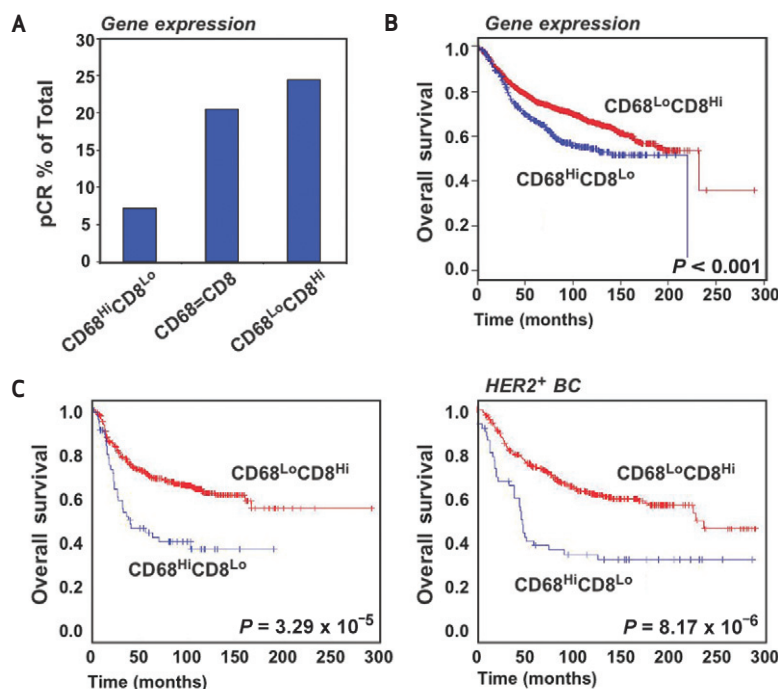
In a previous study, we reported that T-helper 2 (T<sub>H</sub>2)-CD4<sup>+</sup> T-effector cells regulate TAM bioactivity and thereby promote late-stage mammary carcinogenesis and development of pulmonary metastasis (11). We now extend these findings and demonstrate that the complexity of CD8<sup>+</sup> T lymphocytes, CD4<sup>+</sup> T lymphocytes (presumably T<sub>H</sub>2 or T regulatory cells or both), and CD68<sup>+</sup> TAMs is a predictive biomarker for OS and RFS in node-positive breast cancer (Fig. 1). Retrospective clinical studies have previously revealed that the ratio of CD4<sup>+</sup> to CD8<sup>+</sup> T lymphocytes, or T<sub>H</sub>2 to T<sub>H</sub>1 CD4<sup>+</sup> T cells, infiltrating breast cancer correlates with increased tumor grade, lymph node metastasis, and

reduced OS (31). Unsupervised expression profiling of breast cancer-associated stroma revealed a gene signature predictive of good prognostic outcome (>98% 5-year survival) that was functionally enriched for genes suggestive of CTL and natural killer cell activity (32). Moreover, elucidation of a CSF1-response gene expression signature in breast cancer demonstrated that CSF1 signaling correlates with response to therapy and OS (7–9). In this article, we revealed that not only does increased macrophage density correlate with poor outcome (Fig. 1), as reported by others, as well (5, 31, 33), but also the ratio of macrophages/CD68 to CD8<sup>+</sup> T lymphocytes/CD8 $\alpha$  in breast cancer is inversely correlated, an important finding when considering that TAMs can also suppress antitumor immunity. These findings indicate that our immune-based signature may be a useful predictor of recurrence and poor OS for multiple breast cancer subtypes, and, as such, may improve existing gene expression-based prognostic profiling to evaluate risk.

## Breast Cancer CSF1 and CSF1R Expression

Our findings demonstrate that macrophage CSF1R signaling is necessary for their recruitment following induction of CSF1 mRNA and interaction with ligand in carcinoma cells treated with chemotherapy (Fig. 3). Recent studies by Patsialou and colleagues (34) demonstrated that in some human breast carcinoma cell lines, specifically MDA-MB231, steady-state CSF1R mRNA is expressed at high levels and autocrine CSF1-CSF1R signaling enhances invasion (44). Notably, MDA-MB231 cells in our studies did not respond to CTX with increased CSF1 mRNA expression (Fig. 3), likely because these cells already express 10- to 50-fold higher levels of CSF1 mRNA than do other breast cancer cell lines evaluated (data not shown). Carcinoma cells isolated from MMTV-PyMT mice do not express significant levels of CSF1R mRNA (15, 22), indicating that CSF1R blockade in MMTV-PyMT mice influences myeloid biology, as opposed to MECs.

**Figure 7.** Ratio of CD68 to CD8 predicts patient survival and response to neoadjuvant chemotherapy. **A**, frequency of pCR in a cohort of 311 patients constructed from 2 independent datasets. All patients received FNAs prior to neoadjuvant chemotherapy and pathologic response was assessed at definitive surgery. With median expression as a threshold, examination of CD8 $\alpha$  and CD68 mRNA in FNA samples revealed 3 separate groups: CD68 > CD8, CD68 < CD8, and CD68 = CD8 (denoted CD68<sup>high</sup>/CD8<sup>low</sup>, CD68<sup>low</sup>/CD8<sup>high</sup>, and CD68/CD8<sup>equal</sup>, respectively). Analysis of the rate of pCR in the groups is shown. **B**, Kaplan-Meier estimate of survival, comparing CD68<sup>high</sup>/CD8<sup>low</sup> and CD68<sup>low</sup>/CD8<sup>high</sup> immune profiles as assessed by mRNA expression from 3,872 patient samples assembled from 14 different platforms. Median expression for both CD8 and CD68 was used to determine high and low groups within each of the 22 individual datasets. Once a sample was assigned to a particular group, the 22 datasets were combined and a global survival analysis was performed. The log-rank (Mantel-Cox) P value is shown for difference in survival. **C**, Kaplan-Meier estimate of survival, comparing CD68<sup>high</sup>/CD8<sup>low</sup> and CD68<sup>low</sup>/CD8<sup>high</sup> immune profiles as assessed by mRNA expression from 3872 patient samples for tumors stratified into basal and HER2<sup>+</sup> breast cancer. The log-rank (Mantel-Cox) P value is shown for difference in survival.



## Immunosuppressive Macrophages and Chemosensitivity

Development and progression of pulmonary metastases in mammary carcinoma is impaired in mice containing a recessive null mutation in the *CSF1* gene (15, 35). Similarly, blockade of CSF1R signaling impairs aspects of mammary carcinogenesis (36) and metastases (37). We used  $\alpha$ CSF1 mAb and PLX3397, a novel small-molecular-weight tyrosine kinase inhibitor, to efficiently deplete CD11b<sup>+</sup>Ly6G<sup>-</sup>Ly6C<sup>low</sup>F4/80<sup>+</sup> TAMs (70%) without altering the presence of CD11b<sup>+</sup>Ly6G<sup>high</sup>F4/80<sup>-</sup> iMCs or perivascular F4/80<sup>+</sup> macrophages in mammary tumor stroma (Fig. 3).

Malignant mammary epithelial cells from MMTV-PyMT mice express high levels of CSF1, which directly regulates TAM recruitment (and EGF expression) and induction of macrophage HIF1 $\alpha$  (11, 38, 39). We previously reported that IFN- $\gamma$ <sup>+</sup> CD8<sup>+</sup> CTL activity is impaired by myeloid-derived ARG1 and nitric oxide synthase that is HIF1 $\alpha$ -dependent (38). Thus, on the basis of inverse correlation between TAMs and CD8<sup>+</sup> T cells in human breast cancer, and the fact that TAMs infiltrating mammary carcinomas directly suppress CTL activity in a HIF1 $\alpha$ -dependent manner (38), we postulated that TAM depletion would foster antitumor immunity by relieving TAM-mediated CTL suppression and thereby enhance response to cytotoxic therapy. Accordingly, combined treatment of MMTV-PyMT mice with PTX, and either  $\alpha$ CSF1 mAb or PLX3397, slowed primary tumor development, reduced development of high-grade carcinomas (Fig. 4), and decreased pulmonary metastasis by 85% (Fig. 6), features of mammary carcinogenesis accompanied by decreased vascular density (Fig. 4), and increased CD4<sup>+</sup> and CD8<sup>+</sup> T-cell infiltration in primary tumors (Fig. 5). Increased presence of CD8<sup>+</sup> T cells was significant in this regard, as when specifically depleted, the added benefit of combined PLX3397/PTX therapy was lost (Fig. 6).

Immunosuppressive myeloid cells encompass a diverse population of CD11b<sup>+</sup>Gr1<sup>+</sup>Ly6G<sup>+</sup> cells, including myeloid-derived suppressor cells, inflammatory monocytes, neutrophils, and iMCs. Human equivalents have been identified as LIN<sup>low</sup> human leukocyte antigen (HLA)-DR-CD33<sup>+</sup>CD11b<sup>+</sup> and CD14<sup>+</sup>HLA-DR<sup>low</sup> cells (40). CSF1R blockade by PLX3397 depleted CD11b<sup>+</sup>Ly6G<sup>-</sup>Ly6C<sup>low</sup>F4/80<sup>+</sup> TAMs, but not CD11b<sup>+</sup>Ly6G<sup>+</sup> cells (Fig. 3C), which are 12-fold less abundant in MMTV-PyMT carcinomas. In contrast, immunosuppressive CD11b<sup>+</sup>Ly6G<sup>+</sup> cells are more abundant in other mammary tumor models, such as 4T1 (41). This may be an important distinction between tumor types considering the fact that monocyte mobilization from bone marrow is impaired by genetic loss of CSF1, but unaltered following pharmacologic or immunologic inhibition of CSF1R. Gr1<sup>+</sup>CCR2<sup>+</sup>CX3CR1<sup>low</sup> iMCs are highly responsive to CCL2 (42), and CCL2 (MCP1) is expressed at high levels in MMTV-PyMT mammary tumors (Fig. 2C). Therefore, in extrapolating to the clinical scenario, it will be important to stratify human breast cancers containing predominantly high levels of mature tissue TAMs, compared with those containing LIN<sup>low</sup>HLA-DR<sup>-</sup>CD33<sup>+</sup>CD11b<sup>+</sup> or CD14<sup>+</sup>HLA-DR<sup>low</sup> iMCs, because these breast cancers would likely be less responsive to combinatorial therapy involving CSF1R-targeted agents.

## Tissue Specificity and Clinical Implications

Stromal infiltration of TAMs is a poor prognostic indicator for some solid tumor types (43); however, infiltration of TAMs

inside tumor nests, particularly when CD8<sup>+</sup> CTLs are also present, can correlate with improved survival outcome (44). These differences might be explained in part by the fact that TAMs produce either protumor or antitumor bioactivities depending on the types of cytokines to which they are exposed (43). TAMs regulated by T<sub>H</sub>1 cytokines including IFN- $\gamma$ , TNF- $\alpha$ , and granulocyte monocyte colony stimulating factor enhance TAM cytotoxic activity, production of proinflammatory cytokines, and antigen presentation (45). In contrast, tissue macrophages exposed to T<sub>H</sub>2 cytokines, immune complexes, or immunosuppressive cytokines instead block CTL activity and promote angiogenesis and tissue remodeling (43, 45). In non-small cell lung cancer, TAMs that localize to tumor nests and correlate with favorable clinical outcomes exhibit an M1/T<sub>H</sub>1 cytokine profile and express high levels of HLA-DR (46, 47). In contrast, CD163 and CD204 expressing TAMs (M2/T<sub>H</sub>2 markers) correlate with poor clinical outcomes in melanoma, non-small cell lung cancer, and pancreatic cancer (48, 49). We found that tumor tissue from PLX3397/PTX-treated mice had increased *IL12p35* and *IFN $\alpha$ 1* mRNA expression, indicative of bolstered antitumor immunity, indicating that PLX3397/PTX therapy fostered a general reprogramming of the immune microenvironment, in addition to blocking TAM infiltration that together favored CD8<sup>+</sup> T-cell-mediated tumor suppression. Data presented herein do not reveal whether the improved outcome for tumor-bearing mice or the antitumor immune microenvironment fostered under these conditions resulted directly from reduced presence of alternatively activated TAMs, decreased vessel density, or a combination of the two. Given the fact that PLX3397 as monotherapy efficiently reduced TAM presence but had no effect on vessel density, primary carcinoma (Fig. 4), or pulmonary metastasis development (Fig. 6), it seems reasonable to speculate that TAM depletion resulted in loss of an important epithelial cell survival pathway (possibly mediated by EGF) that resists chemotherapy-induced cell death; certainly, however, effects on vascular pathways may also play a role, as has been recently reported by Rolny and colleagues (50). It will be interesting to determine whether directly reprogramming TAMs—for example, by neutralization of IL-4—to favor the presence of classically activated (M1) TAMs, as we have previously reported (11), also similarly enhances antitumor immune programs and chemosensitivity and, if so, whether those responses are also CD8<sup>+</sup> T-cell-dependent.

Microtubule inhibitors constitute one of the most effective classes of cytotoxic agents available for treating both early- and late-stage breast cancer, and are considered the standard of care for treatment of metastatic disease. Several agents that affect microtubule dynamics are active antitumor agents and induce polymerization or cause nonfunctional tubulin aggregates. These compounds block cell division by interfering with function of the mitotic spindle and consequently result in cell-cycle arrest and cell death. PTX is among the most widely used agents in this class. Despite the clinical activity of taxanes, median time to progression in patients treated with PTX is only 6 to 9 months in the first- and second-line setting, and 3 to 4 months in patients with previous exposure to taxanes (51). Although addition of the antiangiogenic agent bevacizumab to PTX improved response and time to progression, it was without impact on OS (52). Glucocorticoid premedication is required for PTX to prevent increased bone marrow and peripheral nerve toxicity as well as allergic reactions and anaphylaxis due to the Cremaphor solvent base. For other cytotoxic agents, glucocorticoids are also commonly used to prevent

toxicities such as nausea, vomiting, and fluid retention. Although these agents are standard additions to many chemotherapies, they suppress production of proinflammatory cytokines and chemokines, severely impair differentiation of antigen presentation by DCs, suppress development of  $T_H1$  cells, and bias immune responses toward  $T_H2$  cell types (53). Our neoadjuvant studies in MMTV-PyMT and orthotopic tumor-bearing mice were performed without dexamethasone, an  $H_2$  antagonist, or diphenhydramine. Thus, it is possible that the  $CD8^+$  T-cell-dependent antitumor program fostered by combined PLX3397/PTX would have been dampened in the presence of dexamethasone. An understanding of the mechanisms that lead to inadequate or poor response to taxanes is urgently needed, as are prognostic biomarkers that predict which patients will respond favorably. That said, it seems reasonable that administration of cytotoxic agents not requiring steroids, in combination with novel strategies such as TAM ablation (or TAM reprogramming), which together bolster natural antitumor immunity, would improve outcomes and extend long-term survival for patients with breast cancer, as well as other cancer types. The clinical outcome of pharmacologically (or immunologically) targeting TAMs directly or the pathways that regulate their recruitment must be considered carefully because all cancer types may not respond in a similar fashion. This study provides a compelling rationale for clinical evaluation of combinatorial therapies inhibiting TAM recruitment, in combination with standard-of-care chemotherapy for treatment of breast cancer, and underscores the importance of identifying a population of patients who, by virtue of their immune profile and CSF1R status, may benefit most from such therapies.

## METHODS

### Patients and Tumor Samples

Tissue microarray studies were conducted on 2 separate patient cohorts. The screening cohort, Cohort I, described elsewhere in detail (54), was constructed from 179 cases of invasive breast cancer diagnosed at the Department of Pathology, Malmö University Hospital, Malmö, Sweden, between 2001 and 2002. The median age at diagnosis was 65 years of age, and the median follow-up time for OS was 52 months. Patients had not received neoadjuvant therapy and were treated with either modified radical mastectomy or wide local excision. The median tumor size was 2.2 cm; 62% of the tumors were PR-positive and 72% were ER-positive. Complete endocrine treatment data were available for 143 patients, 67 of whom received adjuvant tamoxifen, 3 an aromatase inhibitor, and 25 a combination of tamoxifen and an aromatase inhibitor. Information on adjuvant chemotherapy was available for 143 patients, of whom 30 received treatment. The second (validation) cohort, Cohort II, included 498 patients with primary invasive breast cancer diagnosed at the Malmö University Hospital between 1988 and 1992. These cases belonged to an original cohort of 512 patients, as previously described in detail (55). The median age at diagnosis was 65 years, and median follow-up time to first breast cancer event was 128 months. Information regarding the date of death was obtained from regional cause-of-death registries for all patients in both cohorts. Complete endocrine treatment data were available for 379 patients, 160 of whom received adjuvant tamoxifen. Information on adjuvant chemotherapy was available for 382 patients, of whom 23 received treatment. To assemble tissue microarrays, clearly defined areas of tumor tissue were indicated on a slide with a fresh tissue section from the paraffin block. Two biopsy samples, 1.0 mm in diameter, were taken from each donor paraffin block corresponding to the marked area. Recipient blocks were limited to ~200 cores each. In general, cores were taken from the peripheral aspect of the tumor. Necrotic tissue was avoided. For IHC analyses, 4.0- $\mu$ m paraffin sections were used. The ethical committee at Lund University (Malmö, Sweden) approved this study.

### Automated Image Acquisition, Management, and Analysis

Fully automated image acquisition was used for the results presented in this article. The Aperio ScanScope XT Slide Scanner (Aperio Technologies) was used to capture whole-slide digital images with a 20 $\times$  objective. Slides were dearrayed to visualize individual cores, using Spectrum software (Aperio). A tumor-specific nuclear algorithm (IHC-MARK) developed in house was modified to quantify CD4, CD8, and CD68 expression. IHC-MARK was initially designed to identify tumor cells on the basis of nuclear morphologic features (56); however, this was modified for evaluating leukocyte infiltration based on specific nuclear morphologic features.

### Image and Statistical Analysis

A decision tree-supervised algorithm was used to group patients based on immune cell IHC density. For decision tree analysis, all patients were randomly divided into 10 subsets. A decision tree model was selected using a 10-fold cross-validation approach (16). Ten consecutive decision tree models were independently constructed with the immune cell infiltration density continuous output from 9 subsets. Survival outcome predictive power of each decision tree model was tested on the remaining set of patients, and the model with the higher accuracy was selected as optimal for the dataset. Kaplan-Meier analysis and the log-rank test were used to illustrate differences between OS and RFS according to individual CD68, CD4, and CD8 expression. A Cox regression proportional hazards model was used to estimate the relationship to OS of the CD68/CD4/CD8 immune profile; lymph node status; tumor grade; and HER2, PR, and ER status in the patient cohorts. A  $P$  value of  $<0.05$  was considered statistically significant, and calculations were assessed using Statistical Package for the Social Sciences (SPSS, Inc.).

### Neoadjuvant Cohort

The neoadjuvant cohort consisted of 2 gene expression cohorts representing 311 patients treated with neoadjuvant chemotherapy (26, 27), with complete pathologic response in 60 (19%) patients. The majority of patients received PTX and fluorouracil-doxorubicin-cyclophosphamide. Both datasets were examined on the same array platform (Affymetrix U133A), using a standard operating procedure and normalization method (dCHIP) as previously reported (57, 58). Data were downloaded from the Gene Expression Omnibus (59) and an institutional website (60). Normalized expression values for both CD8 and CD68 were established as previously described (54).

### Preclinical Mouse Models and Animal Husbandry

Mice harboring the PyMT transgene under the control of the MMTV promoter in the FVB/n strain were obtained from Dr. Zena Werb [University of California, San Francisco (UCSF), San Francisco, California] and have been previously described (14). Two murine models of mammary tumor development were used to analyze response to chemotherapy (Supplementary Fig. S3). The first model used MMTV-PyMT mice (Supplementary Fig. S3A). The 80-day-old MMTV-PyMT female littermates were randomized by initial tumor volume and fed either PLX3397 (20, 61, 62) formulated in mouse chow or control chow (provided by Plexikon Inc). PLX3397 was formulated in mouse chow so that the average dose per animal per day was 40 mg/kg. When PLX3397-treated MMTV-PyMT mice reached 85 days of age, they were then administered PTX (Hospira) every 5 days by i.v. injection into the retroorbital plexus. PTX was given at 10 mg/kg of the animal per injection, diluted in PBS. Tumor burden was evaluated by caliper measurement every 5 days following the start of PLX3397 treatment. Prior to tissue collection, mice were cardiac-perfused with PBS to clear peripheral blood. Mammary tumor tissue from PBS-perfused MMTV-PyMT mice was analyzed by flow cytometry and qRT-PCR 2 days after the second dose of PTX, when metastatic burden and tumor grade were determined. Primary tumor burden was determined by caliper measurements on live sedated mice. Metastatic burden was assessed by serial sectioning of formalin-fixed paraffin-embedded lung tissue whereby the entire lung was sectioned and the number of metastatic foci ( $>5$  cells) was determined on 6 sections taken every 100  $\mu$ m following H&E staining. Lungs from  $>10$  mice/group were analyzed.

To assess tumor grade, the stage characterization technique classified tumor tissue into 3 levels of histologic progression by quantifying the area of transformed glands occupied by each stage (15, 38). Progression follows from a “precancerous stage” characterized by premalignant hyperplasia and adenoma/mouse intestinal epithelium but with the retention of some normal ductal and acinar mammary gland morphology, to a more epithelial cell-dense “early carcinoma” with some stromal invasion, and finally to an invasive, high-mitotic index “late-stage carcinoma.”

The IHC analysis was conducted on tissue sections following the end of studies on 100-day-old MMTV-PyMT mice (detailed in Supplementary Fig. S4A). Vehicle-treated mice received PBS-only injections. We also used a syngeneic orthotopic implantable tumor model (referred to as PyMT-implantable in all figures and detailed in Supplementary Fig. S4B). For this model, single-cell suspensions of tumor cell pools isolated from mammary tumors of 3 or 4 100-day-old MMTV-PyMT mice were generated following collagenase A digestion (see discussion of flow cytometry analysis earlier). A total of 1.0 million tumor cells from pools were diluted in medium and basement membrane extract (Matrigel, BD Pharmingen) and injected orthotopically into uncleared mammary fat pads (4th gland) of 10-week-old virgin FVB/n female mice. Following implantation, tumors were allowed to grow to a mean diameter of 1.0 cm before enrollment into studies. Mice were randomized into treatment groups based on tumor size and treated with PLX3397 and PTX, as described above. For some studies, CBDCA (Hospira) was used and administered at 10 mg/kg of mouse per injection, in a similar manner to administration of PTX (see above). For mice with implantable tumors, tumor burden was evaluated by caliper measurement every 2 to 3 days following the start of PLX3397 treatment, and mammary tissue was analyzed by flow cytometry, IHC, and qRT-PCR at the end of the study (Supplementary Fig. S3B). Immune-depleted mice were injected i.p. every 5 days with either 1.0 mg anti-CD8 immunoglobulin G (YTS169.4) or isotype control rat immunoglobulin on day 1 followed by 500 µg every 5 days. All mice were maintained within the UCSF Laboratory for Animal Care barrier facility, and the UCSF Institutional Animal Care and Use Committee approved all experiments involving animals.

Additional information on methods and cohorts is available in the Supplementary Data.

## Disclosure of Potential Conflicts of Interest

E. Rexhepaj, D.J. Brennan, and W.M. Gallagher are inventors of a pending patent application in relation to the development of novel automated image analysis approaches in histopathology, and D.G. DeNardo, D.J. Brennan and L.M. Coussens are inventors of a pending patent application in relation to immune-based signatures for predicting breast cancer risk. B.L. West is an employee of Plexikon Inc. but had no involvement in data collection, analysis, or interpretation.

## Acknowledgments

The authors thank the UCSF Helen Diller Family Comprehensive Cancer Center Laboratory for Cell Analysis and Mouse Pathology shared resource core facilities; members of the Coussens lab for critical discussion; and Plexikon Inc. for providing PLX3397.

## Grant Support

This work was supported by the American Cancer Society and National Cancer Institute Postdoctoral Training Grants (D.G. DeNardo); Department of Defense Breast Cancer Research Program and a Dr. Susan Love Research Foundation Instructional Grant (B. Ruffell); Breast Cancer Research Foundation (H.S. Rugo); and The University College Dublin Conway Institute, which is funded by the Programme for Research in Third Level Institutions, as administered by the Higher Education Authority of Ireland. Funding is acknowledged from Enterprise Ireland (D.J. Brennan, E. Rexhepaj, and W.M. Gallagher); Science Foundation Ireland Strategic Research Cluster award to Molecular Therapeutics for Cancer Ireland (W.M. Gallagher and S.F. Madden); and NIH/National Cancer Institute Grants R01CA130980,

R01CA132566, R01CA140943, and P50CA58207, and the Department of Defense Grants W81XWH-06-1-0416 and PR080717 (L.M. Coussens).

Received November 30, 2010; revised February 7, 2011; accepted February 8, 2011; published OnlineFirst April 3, 2011.

## REFERENCES

- Pollard JW. Trophic macrophages in development and disease. *Nat Rev Immunol* 2009;9:259–70.
- Qian BZ, Pollard JW. Macrophage diversity enhances tumor progression and metastasis. *Cell* 2010;141:39–51.
- Tang R, Beuvon F, Ojeda M, Mosseri V, Pouillart P, Scholl S. M-CSF (monocyte colony stimulating factor) and M-CSF receptor expression by breast tumour cells: M-CSF mediated recruitment of tumour infiltrating monocytes? *J Cell Biochem* 1992;50:350–6.
- Wei S, Nandi S, Chitu V, Yeung YG, Yu W, Huang M, et al. Functional overlap but differential expression of CSF-1 and IL-34 in their CSF-1 receptor-mediated regulation of myeloid cells. *J Leukoc Biol* 2010;88:495–505.
- Campbell MJ, Tonlaar NY, Garwood ER, Huo D, Moore DH, Khramtsov AI, et al. Proliferating macrophages associated with high grade, hormone receptor negative breast cancer and poor clinical outcome. *Breast Cancer Res Treat* 2010 [Epub ahead of print].
- Steidl C, Lee T, Shah SP, Farinha P, Han G, Nayar T, et al. Tumor-associated macrophages and survival in classic Hodgkin's lymphoma. *N Engl J Med* 2010;362:875–85.
- Sharma M, Beck AH, Webster JA, Espinosa I, Montgomery K, Varma S, et al. Analysis of stromal signatures in the tumor microenvironment of ductal carcinoma in situ. *Breast Cancer Res Treat* 2010;123:397–404.
- Espinosa I, Beck AH, Lee CH, Zhu S, Montgomery KD, Marinelli RJ, et al. Coordinate expression of colony-stimulating factor-1 and colony-stimulating factor-1-related proteins is associated with poor prognosis in gynecological and nongynecological leiomyosarcoma. *Am J Pathol* 2009;174:2347–56.
- Beck AH, Espinosa I, Edris B, Li R, Montgomery K, Zhu S, et al. The macrophage colony-stimulating factor 1 response signature in breast carcinoma. *Clin Cancer Res* 2009;15:778–87.
- de Visser KE, Korets LV, Coussens LM. De novo carcinogenesis promoted by chronic inflammation is B lymphocyte dependent. *Cancer Cell* 2005;7:411–23.
- DeNardo DG, Barreto JB, Andreu P, Vasquez L, Tawfik D, Kolhatkar N, et al. CD4(+) T cells regulate pulmonary metastasis of mammary carcinomas by enhancing protumor properties of macrophages. *Cancer Cell* 2009;16:91–102.
- Andreu P, Johansson M, Affara NI, Pucci F, Tan T, Junankar S, et al. Fcγ activation regulates inflammation-associated squamous carcinogenesis. *Cancer Cell* 2010;17:121–34.
- Ammirante M, Luo JL, Grivennikov S, Dedosapov S, Karin M. B-cell-derived lymphotoxin promotes castration-resistant prostate cancer. *Nature* 2010;464:302–6.
- Guy CT, Cardiff RD, Muller WJ. Induction of mammary tumors by expression of polyomavirus middle T oncogene: a transgenic mouse model for metastatic disease. *Mol Cell Biol* 1992;12:954–61.
- Lin EY, Nguyen AV, Russell RG, Pollard JW. Colony-stimulating factor 1 promotes progression of mammary tumors to malignancy. *J Exp Med* 2001;193:727–40.
- Breiman L, Friedman JH, Olshen R, Stone CJ. Classification and regression trees. Pacific Grove, (CA): Wadsworth and Brooks/Cole Advanced Books and Software; 1984.
- DeNardo DG, Andreu P, Coussens LM. Interactions between lymphocytes and myeloid cells regulate pro- versus anti-tumor immunity. *Cancer Metastasis Rev* 2010;29:309–16.
- Gabrilovich DI, Nagaraj S. Myeloid-derived suppressor cells as regulators of the immune system. *Nat Rev Immunol* 2009;9:162–74.
- Haile LA, Gamrekelashvili J, Manns MP, Korangy F, Gretten TF. CD49d is a new marker for distinct myeloid-derived suppressor cell subpopulations in mice. *J Immunol* 2010;185:203–10.
- Artis DR, Bremer R, Gillette S, Hurt CR, Ibrahim PL, Zuckerman RL, Inventors; Plexikon Inc., assignee. Molecular scaffolds for kinase ligand development. United States patent US-20050164300. July 28, 2005.

21. Lin EY, Jones JG, Li P, Zhu L, Whitney KD, Muller WJ, et al. Progression to malignancy in the polyoma middle T oncoprotein mouse breast cancer model provides a reliable model for human diseases. *Am J Pathol* 2003;163:2113–26.
22. Lin EY, Li JF, Gnatovskiy L, Deng Y, Zhu L, Grzesik DA, et al. Macrophages regulate the angiogenic switch in a mouse model of breast cancer. *Cancer Res* 2006;66:11238–46.
23. Lin EY, Pollard JW. Tumor-associated macrophages press the angiogenic switch in breast cancer. *Cancer Res* 2007;67:5064–6.
24. Lin EY, Li JF, Bricard G, Wang W, Deng Y, Sellers R, et al. VEGF testores delayed tumor progression in tumors depleted of macrophages. *Mol Oncol* 2007;1:288–302.
25. Stockmann C, Doedens A, Weidemann A, Zhang N, Takeda N, Greenberg JI, et al. Deletion of vascular endothelial growth factor in myeloid cells accelerates tumorigenesis. *Nature* 2008;456:814–8.
26. Hess KR, Anderson K, Symmans WF, Valero V, Ibrahim N, Mejia JA, et al. Pharmacogenomic predictor of sensitivity to preoperative chemotherapy with paclitaxel and fluorouracil, doxorubicin, and cyclophosphamide in breast cancer. *J Clin Oncol* 2006;24:4236–44.
27. Tabchy A, Valero V, Vidaurre T, Lluh A, Gomez H, Martin M, et al. Evaluation of a 30-gene paclitaxel, fluorouracil, doxorubicin, and cyclophosphamide chemotherapy response predictor in a multicenter randomized trial in breast cancer. *Clin Cancer Res* 2010;16:5351–61.
28. Perou CM, Sorlie T, Eisen MB, van de Rijn M, Jeffrey SS, Rees CA, et al. Molecular portraits of human breast tumours. *Nature* 2000;406:747–52.
29. Sorlie T, Perou CM, Tibshirani R, Aas T, Geisler S, Johnsen H, et al. Gene expression patterns of breast carcinomas distinguish tumor subclasses with clinical implications. *Proc Natl Acad Sci U S A* 2001;98:10869–74.
30. Sorlie T, Tibshirani R, Parker J, Hastie T, Marron JS, Nobel A, et al. Repeated observation of breast tumor subtypes in independent gene expression data sets. *Proc Natl Acad Sci U S A* 2003;100:8418–23.
31. Kohrt HE, Nouri N, Nowels K, Johnson D, Holmes S, Lee PP. Profile of immune cells in axillary lymph nodes predicts disease-free survival in breast cancer. *PLoS Med* 2005;2:e284.
32. Finak G, Bertos N, Pepin F, Sadekova S, Souleimanova M, Zhao H, et al. Stromal gene expression predicts clinical outcome in breast cancer. *Nat Med* 2008;14:518–27.
33. Leek RD, Lewis CE, Whitehouse R, Greenall M, Clarke J, Harris AL. Association of macrophage infiltration with angiogenesis and prognosis in invasive breast carcinoma. *Cancer Res* 1996;56: 4625–9.
34. Patsialou A, Wyckoff J, Wang Y, Goswami S, Stanley ER, Condeelis JS. Invasion of human breast cancer cells in vivo requires both paracrine and autocrine loops involving the colony-stimulating factor-1 receptor. *Cancer Res* 2009;69:9498–506.
35. Nowicki A, Szenajch J, Ostrowska G, Wojtowicz A, Wojtowicz K, Kruszewski AA, et al. Impaired tumor growth in colony-stimulating factor 1 (CSF-1)-deficient, macrophage-deficient op/op mouse: evidence for a role of CSF-1-dependent macrophages in formation of tumor stroma. *Int J Cancer* 1996;65:112–9.
36. Qian B, Deng Y, Im JH, Muschel RJ, Zou Y, Li J, et al. A distinct macrophage population mediates metastatic breast cancer cell extravasation, establishment and growth. *PLoS One* 2009;4:e6562.
37. Manthey CL, Johnson DL, Illig CR, Tuman RW, Zhou Z, Baker JF, et al. JNJ-28312141, a novel orally active colony-stimulating factor-1 receptor/FMS-related receptor tyrosine kinase-3 receptor tyrosine kinase inhibitor with potential utility in solid tumors, bone metastases, and acute myeloid leukemia. *Mol Cancer Ther* 2009;8:3151–61.
38. Doedens AL, Stockmann C, Rubinstein MP, Liao D, Zhang N, Denardo DG, et al. Macrophage expression of hypoxia-inducible factor-1 $\alpha$  suppresses T-cell function and promotes tumor progression. *Cancer Res* 2010;70:7465–75.
39. Wyckoff J, Wang W, Lin EY, Wang Y, Pixley F, Stanley ER, et al. A paracrine loop between tumor cells and macrophages is required for tumor cell migration in mammary tumors. *Cancer Res* 2004;64:7022–9.
40. Serafini P, Borrello I, Bronte V. Myeloid suppressor cells in cancer: recruitment, phenotype, properties, and mechanisms of immune suppression. *Semin Cancer Biol* 2006;16:53–65.
41. Bunt SK, Yang L, Sinha P, Clements VK, Leips J, Ostrand-Rosenberg S. Reduced inflammation in the tumor microenvironment delays the accumulation of myeloid-derived suppressor cells and limits tumor progression. *Cancer Res* 2007;67:10019–26.
42. Zhang J, Patel L, Pienta KJ. CC chemokine ligand 2 (CCL2) promotes prostate cancer tumorigenesis and metastasis. *Cytokine Growth Factor Rev* 2010;21:41–8.
43. Ruffell B, Denardo DG, Affara NI, Coussens LM. Lymphocytes in cancer development: polarization towards pro-tumor immunity. *Cytokine Growth Factor Rev* 2010;21:3–10.
44. Kawai O, Ishii G, Kubota K, Murata Y, Naito Y, Mizuno T, et al. Predominant infiltration of macrophages and CD8(+) T cells in cancer nests is a significant predictor of survival in stage IV nonsmall cell lung cancer. *Cancer* 2008;113:1387–95.
45. Mantovani A, Locati M. Orchestration of macrophage polarization. *Blood* 2009;114:3135–6.
46. Ma J, Liu L, Che G, Yu N, Dai F, You Z. The M1 form of tumor-associated macrophages in non-small cell lung cancer is positively associated with survival time. *BMC Cancer* 2010;10:112.
47. Ohri CM, Shikotra A, Green RH, Waller DA, Bradding P. Macrophages within NSCLC tumour islets are predominantly of a cytotoxic M1 phenotype associated with extended survival. *Eur Respir J* 2009;33:118–26.
48. Bronkhorst IH, Ly LV, Jordanova ES, Vrolijk H, Versluis M, Luyten GP, et al. Detection of M2 macrophages in uveal melanoma and relation with survival. *Invest Ophthalmol Vis Sci* 2011;52:643–50.
49. Kurahara H, Shinchi H, Mataka Y, Maemura K, Noma H, Kubo F, et al. Significance of M2-polarized tumor-associated macrophage in pancreatic cancer. *J Surg Res* 2009 [Epub ahead of print].
50. Rolny C, Mazzone M, Tugues S, Laoui D, Johansson I, Coulon C, et al. HRG inhibits tumor growth and metastasis by inducing macrophage polarization and vessel normalization through downregulation of PlGF. *Cancer Cell* 2011;19:31–44.
51. Twelves C, Cortes J, Vahdat LT, Wanders J, Akerele C, Kaufman PA. Phase III trials of eribulin mesylate (E7389) in extensively pretreated patients with locally recurrent or metastatic breast cancer. *Clin Breast Cancer* 2010;10:160–3.
52. Miller K, Wang M, Gralow J, Dickler M, Cobleigh M, Perez EA, et al. Paclitaxel plus bevacizumab versus paclitaxel alone for metastatic breast cancer. *N Engl J Med* 2007;357:2666–76.
53. Zitvogel L, Kroemer G. The dilemma of anticancer therapy: tumor-specific versus immune effects. *Blood* 2008;112:4364–5.
54. Brennan DJ, Rexhepaj E, O'Brien SL, McSherry E, O'Connor DP, Fagan A, et al. Altered cytoplasmic-to-nuclear ratio of survivin is a prognostic indicator in breast cancer. *Clin Cancer Res* 2008;14:2681–9.
55. Paulsson J, Sjoblom T, Micic P, Ponten F, Landberg G, Heldin CH, et al. Prognostic significance of stromal platelet-derived growth factor beta-receptor expression in human breast cancer. *Am J Pathol* 2009;175:334–41.
56. Rexhepaj E, Brennan DJ, Holloway P, Kay EW, McCann AH, Landberg G, et al. Novel image analysis approach for quantifying expression of nuclear proteins assessed by immunohistochemistry: application to measurement of oestrogen and progesterone receptor levels in breast cancer. *Breast Cancer Res* 2008;10:R89.
57. Mazouni C, Peintinger F, Wan-Kau S, Andre F, Gonzalez-Angulo AM, Symmans WF, et al. Residual ductal carcinoma in situ in patients with complete eradication of invasive breast cancer after neoadjuvant chemotherapy does not adversely affect patient outcome. *J Clin Oncol* 2007;25:2650–5.
58. Moody SE, Perez D, Pan TC, Sarkisian CJ, Portocarrero CP, Sterner CJ, et al. The transcriptional repressor Snail promotes mammary tumor recurrence. *Cancer Cell* 2005;8:197–209.
59. Gene Expression Omnibus [database on the Internet]. Bethesda (MD): National Center for Biotechnology Information/National Library of Medicine/NIH. 2010 [cited 2011]. Available from <http://www.ncbi.nlm.nih.gov/geo/query/acc.cgi?acc=GSE20271>
60. Department of Bioinformatics and Computational Biology [database on the Internet]. Houston (TX): The University of Texas MD Anderson Cancer Center. 2003 [cited 2011]. Available from <http://bioinformatics.mdanderson.org/pubdata.html>
61. Tsai J, Lee JT, Wang W, Zhang J, Cho H, Mamo S, et al. Discovery of a selective inhibitor of oncogenic B-Raf kinase with potent antimelanoma activity. *Proc Natl Acad Sci U S A* 2008;105:3041–6.
62. Louvet C, Szot GL, Lang J, Lee MR, Martinier N, Bollag G, et al. Tyrosine kinase inhibitors reverse type 1 diabetes in nonobese diabetic mice. *Proc Natl Acad Sci U S A* 2008;105:18895–900.